CDF/DOC/SEC_VTX/PUBLIC/4924

Proposal for a Very Low Mass, Very Small Radius Silicon Layer In the CDF II Upgrade*

P. Azzi-Bacchetta†, N. Bacchetta†, F. Dejongh‡, J. Goldstein‡, C.Haber§, M. Hrycyk‡, J. Incandela‡, C.M. Lei‡, G. Martignon**, F. Snider‡, D. Stuart‡

August, 1998

ABSTRACT

We propose the construction and installation of a layer of silicon microstrips at very small radius. The additional layer would improve track purity and result in more precise and uniform track impact parameter measurements by CDF II with corresponding improvements in high p_T b tagging and overall pattern recognition that would result in greater sensitivity to a low mass higgs. It would also improve performance of CDF II for B physics and SUSY searches. The basic readout element would be individual, single sided, axial strip sensors ~10 cm long. A readout pitch of 50 μm *is considered along with the possibility of alternating strips for an overall 25* μm *pitch to provide hit position resolution of order –6* μm*. The sensors take advantage of recent LHC designs for high bias voltages that enable good signal-to-noise ratios after extreme radiation doses. Layer 00 would be expected to significantly outlive the innermost layer of SVX II despite a two-fold greater radiation exposure rate. It would thus allow the possibility of extended high p_T data taking. It would also provide CDF experience with new radiation hard microstrip detectors that could lead to a straightforward upgrade of the inner layers of SVX II for Run III with minimal downtime. Thus, Layer 00 is the first step toward maximizing CDF II data taking with a commensurate enhancement of the ability of CDF II to detect a low mass higgs or SUSY signal in the pre-LHC era. The overall costs, manpower, and schedule for the construction of Layer 00 are reasonable and achievable within the CDF II upgrade schedule.*

---

* Presented to the CDF Beyond the Baseline Committee, July 1998, and the PAC, October 1998.
† INFN-Padova
‡ Fermilab
§ LBNL
** Purdue

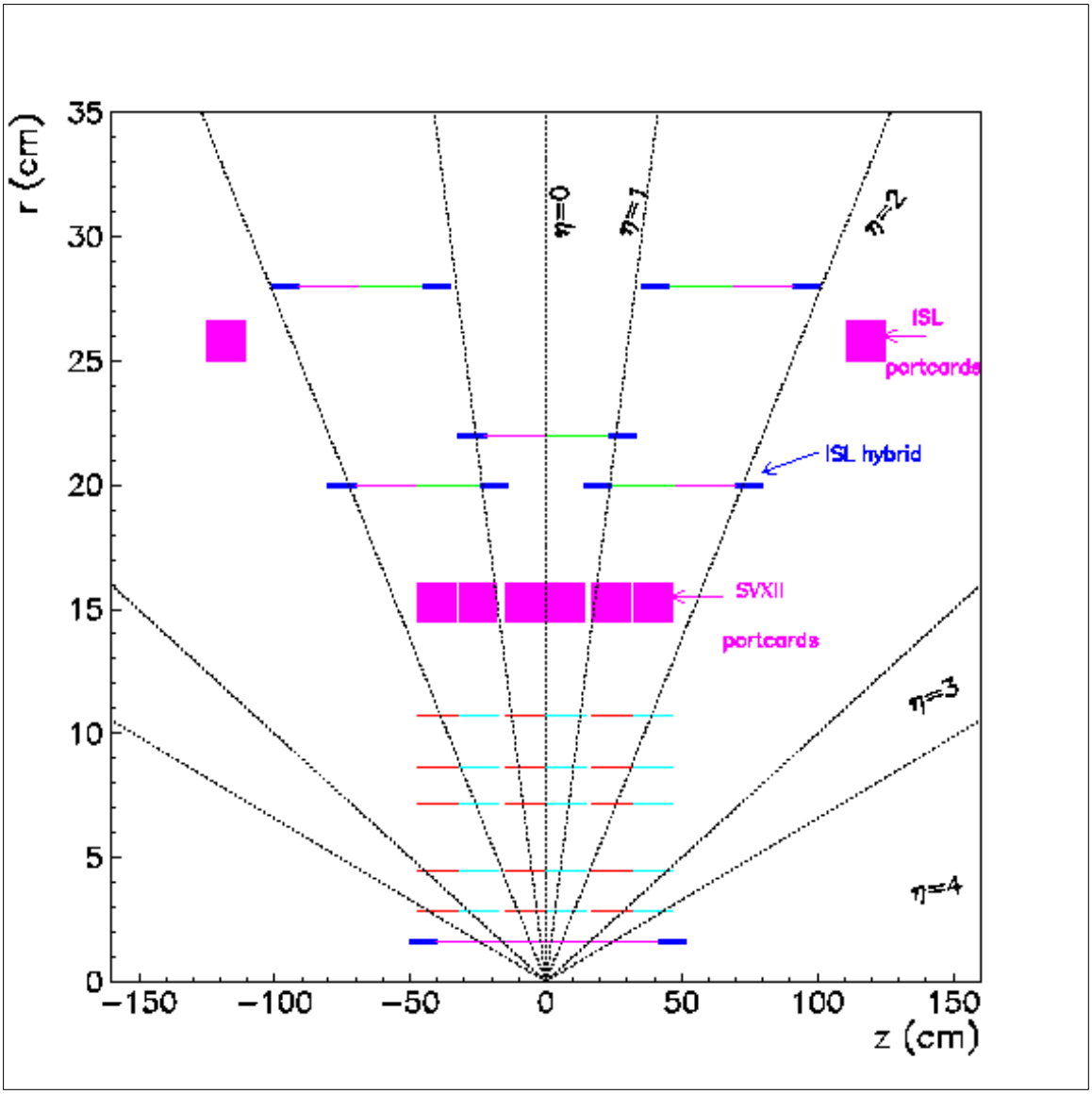

Figure 1: Schematic layout of the CDF II silicon tracker, with Layer 00 at a radius of 1.6 cm. The radial scale is expanded to display the silicon layers more clearly.

1. Introduction

The CDF II tracking system will produce major improvements in our ability to b tag, flavor tag, and reconstruct B hadron decays. We expect higher tracking efficiency and purity than was the case in Run I[1]. The combination of a highly compact SVXII silicon vertex detector and the increased length of all silicon layers, including those of the large radius ISL silicon tracker, will result in a large increase in b daughter track acceptance. The CDF Run II silicon tracking system thus overcomes the main weaknesses of the Run I system.

The Run II tracker does however have a few vulnerabilities. Exceptional track acceptance is achieved at the expense of increasing the mass of the active layers. As a result, the impact parameter resolution of the Run II silicon vertex detector for low momentum tracks is degraded over large regions of the detector. A second vulnerability of the CDF tracking system is that it doesn't have a clear upgrade path. The innermost layers of SVXII will be exposed to large amounts of radiation and should survive the upcoming run,[2,3,4] but will need to be replaced for Run III. This presents problems of timing and resources. The only meaningful time for Run III to occur is before the LHC detectors begin to produce physics. A significant portion of this window of opportunity will be lost when CDF disassembles to repair SVXII.[††] *This should happen only once and for the shortest possible amount of time.*

While pondering these issues, we were driven to investigate the possibility of a low mass, small radius, silicon microstrip detector, which we refer to as Layer 00 (abbr. L00). If such a system could be designed, installed, and operated in Run II, a small flock of birds would be killed with one stone. We now present the outcome of our study of the potential and difficulties associated with a beampipe silicon layer for Run II.

2. Motivation

One motive for installing a layer of silicon at a very small radius is obvious: better impact parameter resolution, leading to improvements in b tagging and B physics. Indeed, we will show that the improvement is rather dramatic, not only in the regions where the SVXII innermost layer hybrids reside, but *everywhere*.

A key element to meeting the challenge of building Layer 00 is the availability of extreme radiation tolerant (rad-hard) silicon microstrip detectors. These detectors are expected to withstand annual doses of ~1 Mrad for as long as a decade. This brings us to several other reasons for our proposal. With an innermost layer having such high radiation tolerance, CDF is less vulnerable to the loss of the SVXII inner layers and is in a better position to upgrade for Run III. If the inner layer of SVXII dies prematurely, for example, we may lose some of our hadronic b triggering capability[‡‡], but a small radius, extremely rad-hard layer would guarantee continued high quality data for some time. This would be especially useful if we happen to see the hint of a major new discovery.

The current options for inner layer replacements[5] are pixels, diamonds, and rad-hard silicon microstrip detectors. While pixels (either silicon or diamond) would give potentially outstanding radiation hardness and pattern recognition capability, they also require the most effort, time, and money. It would be a challenge to complete a pixel replacement by the end of Run II. Diamond microstrip detectors, while rad-hard and continually improving in performance,[6] still require some basic R&D and have not been used in large-scale systems. If viable diamond detectors can be produced in large quantities in the next few years, they will be an extremely attractive option. However, diamonds, like pixels, would require a new front-end readout chip.[5]

The only other possibility is rad-hard silicon microstrip detectors. Silicon microstrip detectors with extraordinarily high operating voltage and radiation tolerance have been

[††] A removable innermost section was investigated for SVXII. It is an extremely difficult task as a result of alignment requirements for displaced track triggering.
[‡‡] Investigations are underway to determine if Layer 00 could be included in the SVT trigger.

developed for the major LHC experiments.[7,8,9,10] They have been studied and are well-understood at this time. They could also operate with the existing SVX 3 front-end chip. The main difficulty is that they would need to be kept at low temperatures (0 to -10° C) at almost all times after they have received a significant radiation dose and have undergone type inversion.[11] This is not a significant problem. Moreover, operational experience with these detectors would give us the knowledge and confidence necessary to use them more extensively in Run III. This would assure us of at least one fast upgrade path.

The most exciting reason for installing a small radius layer of silicon is that it would enhance our ability to b tag for top studies and higgs searches, improve our B physics, as for example the measurement of B_s mixing[12], and much more. Other applications are less obvious and cannot be demonstrated as quantitatively because the necessary pattern recognition code doesn't yet exist. The physics case in favor of adding a low mass, and very small radius, high resolution tracking layer is probably as obvious to our CDF collaborators as it is to us. What is less apparent, and where we believe the reader should be most skeptical, regards how such a layer can be implemented. We had a strong initial bias against its feasibility. If it were not for the many problems it would simultaneously solve, we would not have pursued it. We now believe it is achievable for Run II.

2.1 Impact Parameter Resolution

It should be noted that even if one were to argue that the main focus of CDF should be high p_T physics, this would not eliminate the desire for good resolution at low momentum. In Figure 2 we show the momentum distribution of visible charged tracks from b and sequential c hadron decays in top events passing trigger and top group filter requirements. Note that the momentum distribution, while extending to very high values, has a significant low momentum population. Roughly 75 % of the entries lie below 6 GeV.

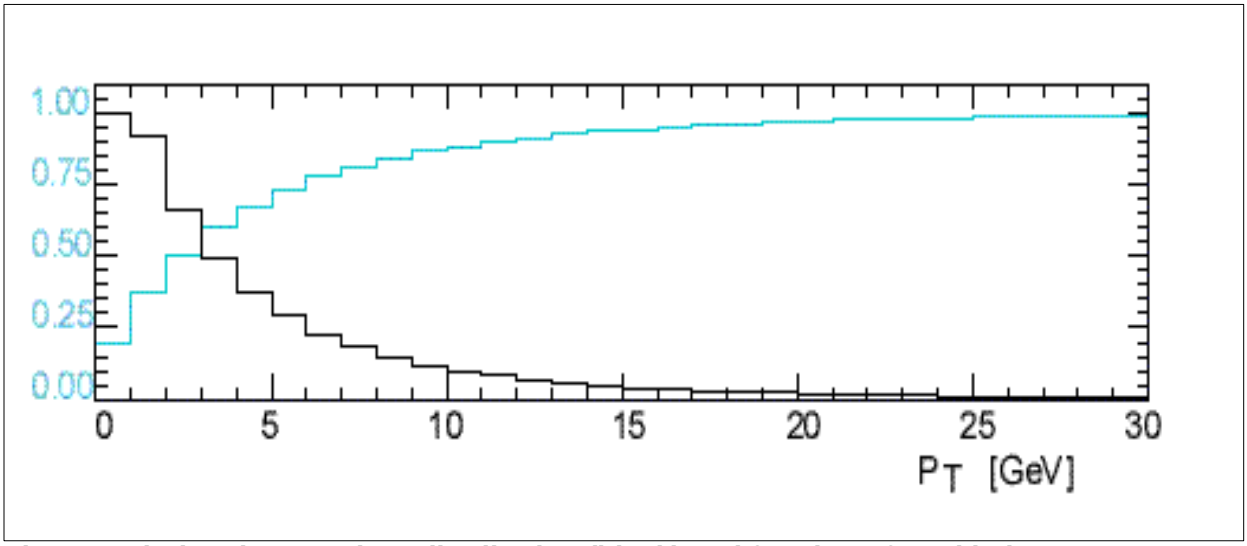

Figure 2. b daughter track p_T distribution (black) and fraction of total below a given p_T (blue) in top decays, (with m_t = 175 GeV/c^2).

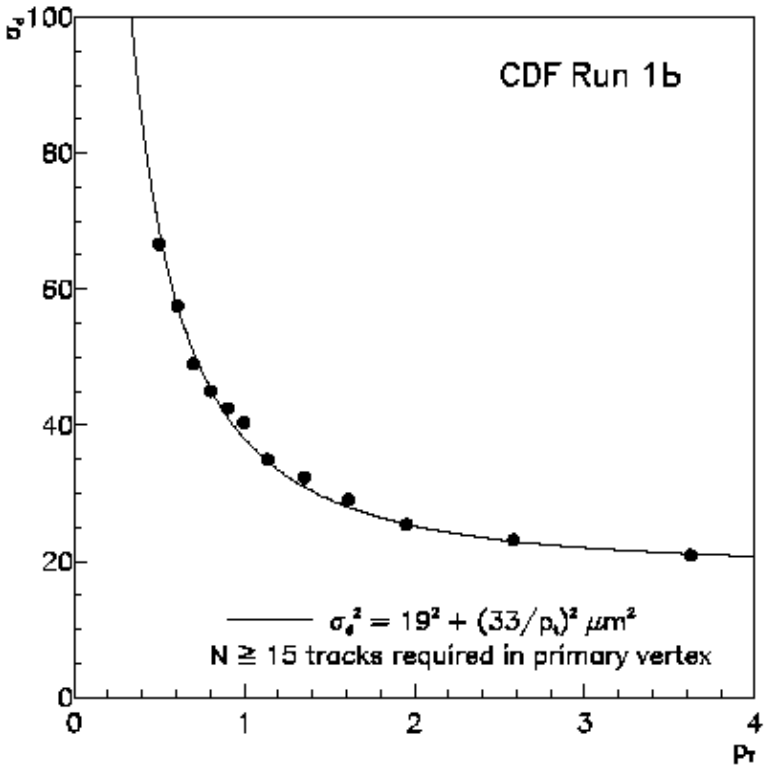

Figure 3. Impact parameter resolution as a function of p_T measured with the CDF SVX′ detector in Run 1b for events with high multiplicity primary vertices.

The low momentum resolution of the CDF SVX and SVX′ detectors was very good, as seen in Figure 3.[13] However, upon calculating the resolution for SVXII, we found that it was degraded for tracks traversing the inner layer electronics hybrids. This is a serious concern because the hybrids cover 33 % of the detector and 50 % of the central $\pm$ 1 σ of the luminous region. Let's review these calculations.

We first calculated[14] SVX′ resolution as a test of the program and obtained

$$\sigma = \sqrt{}\ (13^2 + (34/p_T)^2\ ) \qquad [\mu m]$$

The multiple scattering term is in good agreement with that measured and shown in Figure 3. The asymptotic value of 13 is small compared to the measured value of 19 μm. The discrepancy can be understood as follows. The measured value of 19 includes two effects not incorporated in the calculation. The first is the uncertainty on the primary vertex used to reference the impact parameter measurement. We estimate that for the high multiplicity events that were used, this contribution is of order $\pm$10 μm. The second effect is that due to wedge-to-wedge misalignments in SVX′, which is also on the order of $\pm$ 10 μm. When these are added in quadrature with the calculated value of $\pm$ 13 μm, the result is of order $\pm$20 μm, in agreement with that shown in the figure.

For SVXII, the material budget of each layer has been determined.[15] Table 1 lists the material as a percentage of a radiation length (X_o) and the corresponding impact parameter resolution for tracks traversing various regions of SVXII. Since alternate wedges have different radial positions, we entered two values for each resolution term.

The first set of regions considered is the following:

i) Silicon-only traversed at each layer
ii) Layer 0 silicon-only and silicon + hybrids at all other layers
iii) Layer 0 silicon + hybrids and silicon-only at all other layers
iv) Silicon + hybrids at all layers

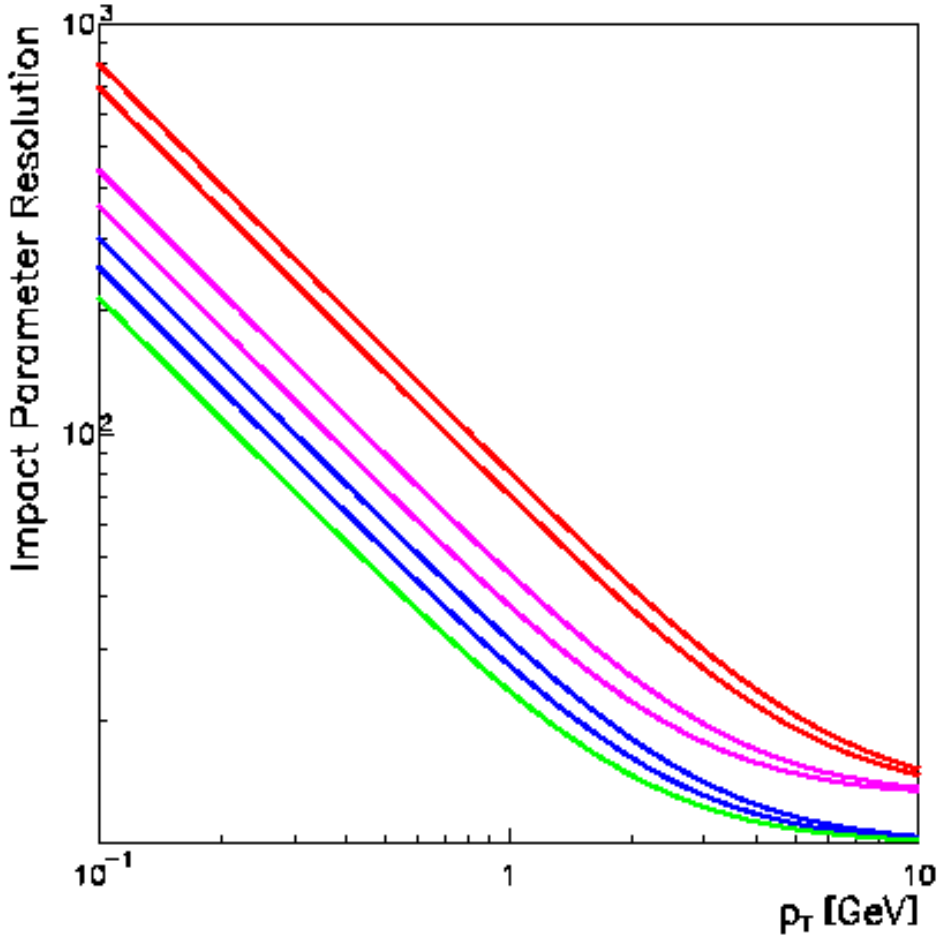

Figure 4. Estimated IP resolutions at low momentum for SVXII bulkhead and hybrid regions (top two red curves), silicon-only regions (next two magenta curves). These become the two blue and the green (bottom) curves, respectively, after adding Layer 00.

This does not exhaust all possible combinations but the tabulated results make it clear that the resolution is predominantly determined by the amount of material traversed in the innermost layer. One can easily bound the results for the missing combinations using those presented in the table.

The second group of regions corresponds to the SVXII bulkheads, which gets roughly 6% of all normally incident tracks. The final set of regions corresponds to the case where tracks hit adjacent overlapped silicon at a given layer. This region was designed to be quite large in SVXII in order to facilitate wedge-to-wedge alignment. It represents roughly 15 % of all normally incident particle trajectories.

Of course normally incident tracks are a small fraction of the total. The exact fraction of tracks traversing the various combinations of layer regions listed in the table will depend on the type of physics in question and the size of the interaction region.

Table 1. SVXII Material and Impact Parameter Resolution $\sigma = \sqrt{A^2 + (B/p_T)^2}$

Layer 0		**Other Layers**		**Resolution**	
Region hit	L0 Mat'l (% X_o)	Region hit	L1 Mat'l (% X_o)	A_a, A_b	B_a, B_b
Silicon	0.38	Silicon	0.36	9, 10	34, 38
Silicon	0.38	Hybrids	2.43	9, 10	41, 46
Hybrids	2.48	Silicon	0.36	9, 10	62, 72
Hybrids	2.48	Hybrids	2.43	9, 10	66, 76
Bulkhead Region					
Region hit	L0 Mat'l (% X_o)	Region hit	L1 Mat'l (% X_o)	A_a, A_b	B_a, B_b
Hybrids	3.48	Silicon	3.63	9, 10	72, 83
Hybrids	3.48	Hybrids	3.43	9, 10	76, 88
Overlap of Layer 0 with Layer 0					
Region hit	L0 & L0 Mat'l	Region hit	L1 Mat'l (% X_o)	A	B
Silicon	0.76	Silicon	0.36	9	39
Silicon	0.76	Hybrids	2.43	9	44
Hybrids	5.0	Silicon	0.36	9	79
Hybrids	5.0	Hybrids	2.43	9	80

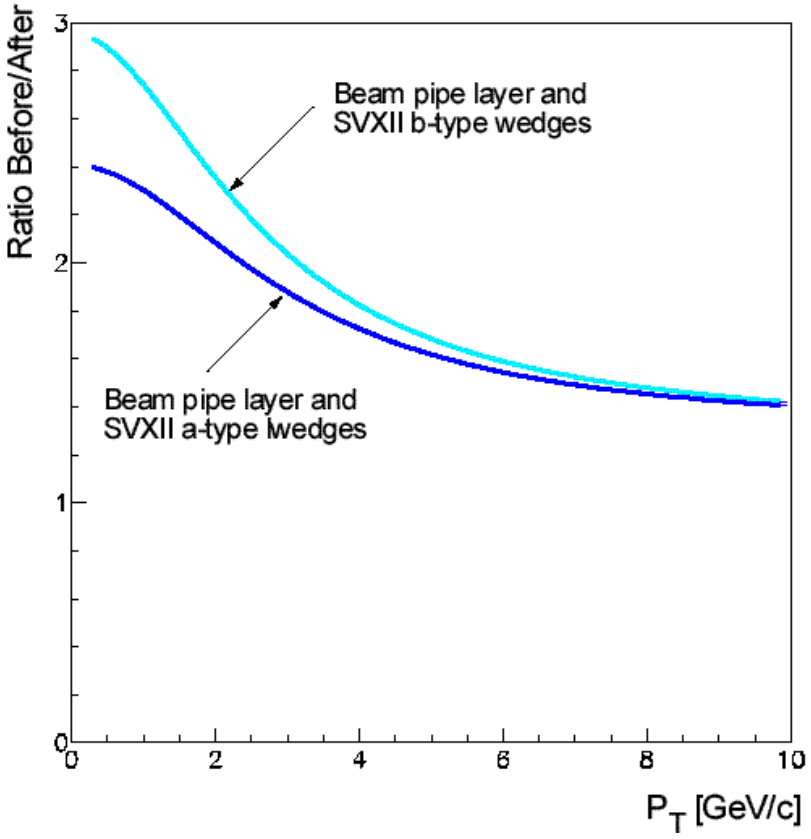

Figure 5. Ratio of impact parameter resolution at the SVXII hybrids before and after installation of Layer 00. The top curve is for Layer 00 combined with the larger radius SVXII wedges (type b).

We conclude that a large part of the SVXII detector acceptance will have worse low momentum resolution than was the case for SVX. More than a third of the track acceptance of SVXII will have a multiple scattering contribution to impact parameter resolution greater than $60/p_T$. The impact parameter resolution at 1 GeV for normally incident tracks is shown in Figure 6. The asymptotic resolution of SVXII will however be very good. The intrinsic asymptotic resolution of 9 - 10 μm will of course not be realized in practice. For extremely high track multiplicity the uncertainty contributed by the primary vertex will be ~ 7 μm.[§§] Improved wedge-to-wedge alignments should reduce the misalignment contribution considerably. We therefore expect the final asymptotic resolution for SVXII in high multiplicity events to be of order 13 μm as compared to 19 μm for SVX′.

[§§] We scaled the result for SVX′ by the ratio of asymptotic resolutions for SVXII and SVX′,

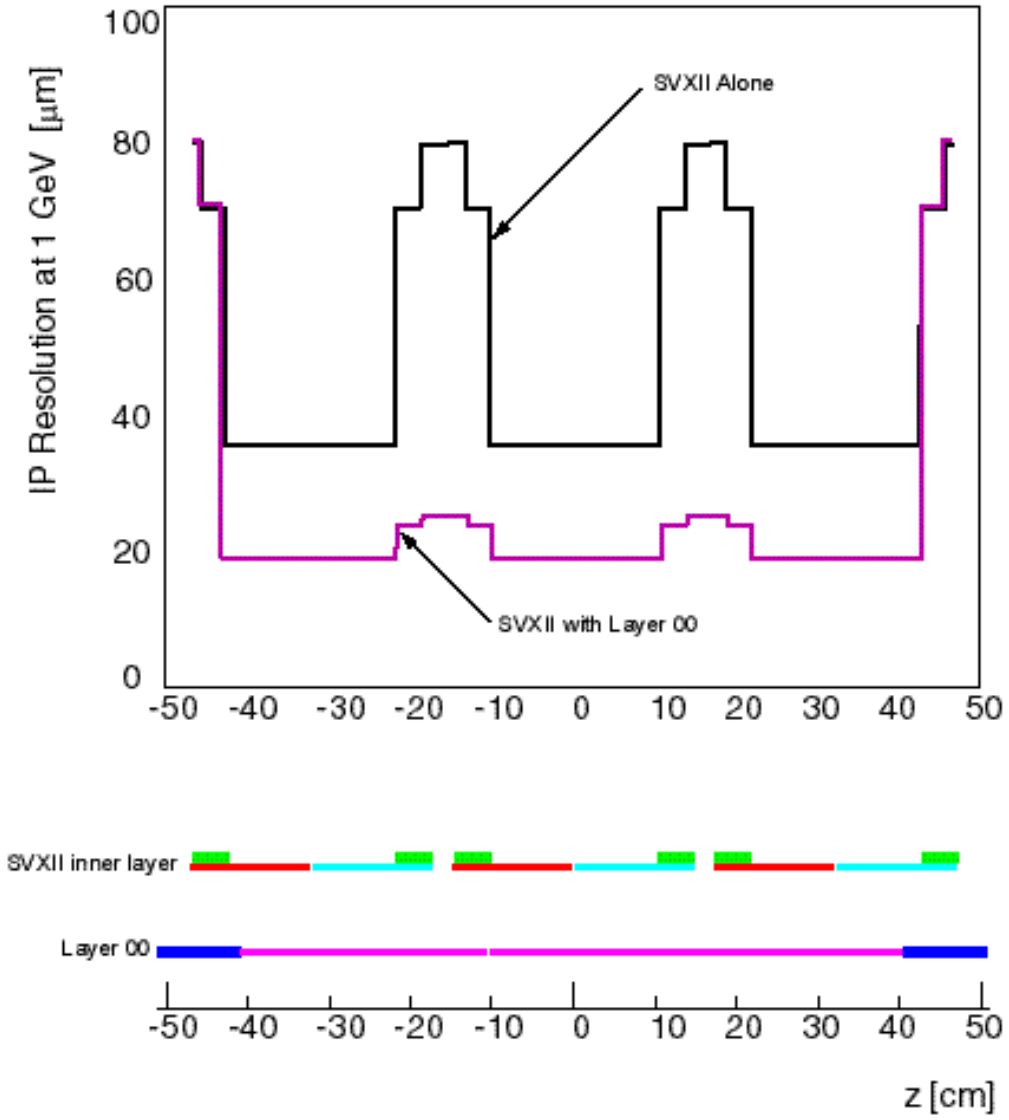

Figure 6. Impact parameter resolution for normally incident 1 GeV/c tracks as a function of z for SVXII and SVXII plus Layer 00 (shown schematically at bottom).

In Table 2 and Figure 6 we show the effect of adding a silicon layer just outside the beampipe with strip pitch of 25 μm. Comparing with Table 1 we see that the effect of Layer 00 is dramatic. In all regions of SVXII, even those of the hybrids and bulkheads combined, the impact parameter resolution is better than it was in the best previous case. As discussed above, the impact parameter resolution in the table is not the resolution that can be achieved in practice. In the case of Layer 00, the contribution to the asymptotic term from the uncertainty in the primary vertex position will be smaller than for SVXII as a result of the better intrinsic resolution. Hence we estimate that the resolution in the region of the SVXII hybrids will be $\sqrt{10^2 + (22/p_T)^2} \leq \sigma \leq \sqrt{10^2 + (27/p_T)^2}$. Figure 5 plots the ratio of resolutions with and without Layer 00 in the region of the layer 0 hybrids, as a function of p_T.

Table 2. Impact parameter resolutions after adding Layer 00.

Layer 0		Other Layers		Resolution	
Region hit	L0 Mat'l (% X_o)	Region hit	L1 Mat'l (% X_o)	A	B
Silicon	0.38	Silicon	0.36	6,7	22,21
Silicon	0.38	Hybrids	2.43	6,7	22,21
Hybrids	2.48	Silicon	0.36	6,7	27,22
Hybrids	2.48	Hybrids	2.43	6,7	27,22
Bulkhead Region					
Region hit	L0 Mat'l (% X_o)	Region hit	L1 Mat'l (% X_o)	A	B
Hybrids	3.48	Silicon	3.63	6,7	32,28
Hybrids	3.48	Hybrids	3.43	6,7	32,28

Finally, we calculated the impact parameter resolution of SVXII for an installed but non-functioning Layer 00. If we do not include Layer 00 in the trigger it is important to see how the added mass will effect the SVT. This also allows one to assess a scenario in which Layer 00 does not function in some regions. We find that in the hybrid regions, the multiple scattering constant B is increased by 1 μm-GeV. In the silicon-only region, it increases by less than 2 μm-GeV. These increases are completely negligible. There is no effect on the asymptotic resolution of SVXII.

In the next several sub-sections we discuss how this improved impact parameter resolution can affect the performance of the CDF II tracking system.

2.2 Purity and Efficiency

Silicon layers have the following characteristics:

1) extremely low probability for noise hits
2) exceptional hit position resolution
3) ~100% probability to form a clear hit signal for charged tracks.

The result is that every additional layer of silicon places very stringent constraints on tracks. By increasing the number of layers of silicon and by requiring that more hit layers be associated to reconstructed tracks, both purity and resolution improves. This was seen very clearly in Run I in a study of optimal track selection for b tagging used in the top search.[16] In that study it was shown that the number of SVX' layers associated with a track was by far the best single indication of track quality. Table 3 summarizes the results for SVXS tracks in Dijet events for which no CTC quality cuts have been applied. Comparing the fractions of observed and expected tracks with n = 2, 3, and 4 layers hit in SVX', it is obvious that those with fewer layers hit have much larger proportions of fakes. This is confirmed by comparing the fraction of tracks which appear to be significantly displaced ($d/\sigma > 3$) to those which are consistent with coming from the primary vertex ($d/\sigma \leq 3$) and noting that one expects ~95 % of the tracks in these events to be prompt. The last row in Table 3 shows that the purity of the 2-hit tracks is extremely low with only 1 in 7 tracks being prompt. This rises to 1 in 2 for 3-hit tracks and 4 of 5 for 4-hit tracks. A similar result was seen while studying standalone tracking with SVXII and ISL.[17] The requirement that a standalone track found with SVXII should point to within ± 2.5 mm of a hit on the inner layer of ISL was found to reduce fake tracks

by roughly a factor of 5. Furthermore, this can be achieved with a negligible reduction in track efficiency.

Table 3. Track quality as a function of the number of SVX' layers hit.

No. of SVX layers hit	2	3	4
Fraction of all SVXS tracks	18 %	25 %	57 %
Fraction Expected from Geometry	4 %	21 %	75 %
Ratio of Prompt to Displaced	1/6	1/1	4/1

The addition of Layer 00 would very likely result in more pure tracking, especially in the forward regions where we intend to rely solely upon silicon for tracking. Higher purity translates into higher efficiency for almost all of the physics we intend to do in Run II. For example, with more fake tracks eliminated, it is possible to loosen b daughter impact parameter significance cuts.

2.3 Physics

- **Overview**

A study has been performed regarding the effect of Layer 00 on the measurement of B_s Mixing.[12] The main conclusion of this study is that our ability to measure x_s depends linearly on proper lifetime resolution which, in turn, is inversely proportional to impact parameter uncertainty. Layer 00 could allow us to probe the entire SM range of x_s values up to 50. We have also calculated Top B tagging using a new parametric detector simulation and tagging program. We find that Layer 00 will improve single tagging by 10 - 15 % and double tagging by 20 – 32 %. Furthermore, if layer 0 of SVXII were to die, the presence of Layer 00 would mean that the tagging efficiencies would be unaffected. For low momentum b jets, SECVTX tagging is increased even more dramatically. With a jet cone of 1.0, and standard cuts, Layer 00 increases double b tagging in b-bbar events by 55%. Layer 00 should however enable lower p_T thresholds to be used. We find that at lower p_T thresholds for which the track resolution with Layer 00 is as good as that of SVXII at standard SECVTX p_T thresholds, the single and double tag efficiencies in b-bbar events increases by 98 % and 280 %, respectively. This will benefit many analyses. For example, it has been shown in run I that SECVTX tagged away-jets yield better flavor dilutions.

- **High P_T Physics**

We have written a Fortran generator-interface program, C++ based parametric detector simulation, and C++ analysis tools. These allow us to generate any desired physics process with Pythia, smear tracks according to chosen detector resolutions to create 3D track parameters with properly corrected covariance matrices, and run the SECVTX tagging algorithm. Output ntuples allow various additional analyses to be performed. The results appear to be reasonable. For instance, we calculate a b tag efficiency of ~49% for b jets completely contained in the active part of SVX'. The Run Ib efficiency obtained for high p_T b jets in Monte Carlo with full detector simulation and reconstruction is ~45 % (see for instance Figure 6 of CDF Note #2989). One expects slightly higher efficiency in our case since there are no detector inefficiencies or pattern recognition errors included.

Briefly summarizing our results; using the SECVTX tagger with standard kinematic cuts, we find that the addition of Layer 00 to SVXII leads to a noticeable enhancement of single and double b-tagging. For b-jets in the SVXII layer 0 hybrid regions, the addition of Layer 00 increases the b tag efficiency by ~ 25 %. In the low mass regions of SVXII, there is an enhancement in the b tag efficiency on the order of 7 %. Overall, the SVXII detector with Layer 00 has a 9% higher single tag efficiency and a 20% higher double tag efficiency than without Layer 00, (assuming a 30 cm luminous region). These results were confirmed by a separate analysis performed by R. Roser.

However, the use of the SECVTX algorithm with standard kinematic cuts may not give a complete picture of the potential improvements we can expect with Layer 00. In particular, since 250 to 750 MeV tracks with Layer 00 will be as well resolved as 500 MeV to 2 GeV tracks in SVXII, it is likely that Layer 00 will enable some reduction in track p_T cuts. Running the SECVTX algorithm with "equivalent p_T thresholds", we find that the addition of Layer 00 leads to a 32 % increase in double b-tagging. (In all cases, a double tag is counted only if both b jets in the event are tagged.)

Finally, one can ask how Layer 00 improves things after SVXII Layer 0 has died. If this occurs with a functioning Layer 00, then there is negligible change in tagging efficiencies. Without Layer 00, there is an 8% reduction in single tagging and 15% reduction in double tagging relative to SVXII. Thus the presence of Layer 00 when Layer 0 dies improves single tagging by 18 to 24 % and double tagging by 42 to 64 %.

Table 4. Comparison of tagging efficiencies.

Detector	B jets Tagged	Equivalent p_T cuts	Single Tags Relative to SVXII	Top events Double tagged	Equivalent p_T cuts	Double Tags Relative to SVXII
SVX'	25.0 ± 0.6%		55 %	8.0 ± 0.5%		38%
SVXII	45.1 ± 0.7%		100%	21.0 ± 0.8%		100%
SVXII – L0 Dead	41.0 ± 0.7%		92.5%	17.8 ± 0.8%		85%
Layer 00	49.3 ± 0.7%	51.8 ± 0.7%	109 to 115 %	25.2 ± 0.8%	27.8 ± 0.6%	120 to 132%

All of the results of our simulations are summarized in Table 4. The percentages of events single and double tagged are relative to all b's in top events and all top events, respectively. Thus, these numbers already include acceptance factors. (For instance, SVX' tagged ~25% of all b's in top events despite a b tag efficiency of ~49 % in our simulation because only half of all b's from top were actually in the detector.)

- **Effects Not Included in Our Simulation**

As mentioned above, these results do not take into account all nuances of real tracking. Pattern recognition errors and failures will diminish the tagging rates tabulated above. Also, additional tracks resulting from interactions of the primary tracks with material in the detector will degrade these numbers. It is not possible to quantify these effects with current tools. The CDF II simulation and tracking should give some idea about these things in future. Nevertheless, it is possible to consider these effects qualitatively.

An additional track hit with high position resolution, as afforded by Layer 00, will result in some reduction in fake tracks and hence allow some increase in track efficiency. On the other side of the coin, it can be argued that Layer 00 adds material to the system and hence increases the secondary track problem. However, the material added by Layer 00 is minimal (0.6 % X_o over most of the coverage). Production of secondary tracks will more likely occur in SVXII (L0 hybrids ~ 2.5% X_o). Layer 00 will, for the most part, only see hits from primary charged particles. This may prove to be invaluable for untangling the effects of secondary particles generated at larger radii.

We expect the tracking system with Layer 00 to be more robust than without it. Hence, any degradation of the tag rates in Table 4 should be equal or smaller in the Layer 00 entries than those cases in which Layer 00 was not included. The case of SVXII with a dead innermost layer is expected to require the greatest downward revision of the tagging numbers tabulated above.

- **Shared hits**

One thing that concerned us was the possibility that many more tracks would overlap in Layer 00 than in SVXII. The innermost radius of Layer 0 is 2.44 cm and the detectors have a pitch of 60 µm. Layer 00 was initially planned to have a radius of 1.7 cm and readout pitch of 50 µm. For these configurations, and considering all tracks with $p_T > 100$ MeV, we asked how many tracks in b jets were within 2 r-ϕ strips of another track. Without taking into account the Z segmentation of Layer 0 and Layer 00, we found that 20% of tracks in Layer 0 and 23 % of tracks in Layer 00 are within 2 strips of another track. This is not a serious increase. More recently, it has been decided to reduce the radius of the CDF II beampipe to 1.2 cm so that the Layer 00 detectors could be placed at a radius of as small as 1.4 cm. In this case, the sharing rises to 27%. However, at this radius we could reduce the number of channels in phi or reduce the pitch in order to make the Layer 00 sensors narrower, in proportion to the reduction in radius. If we were to reduce the pitch to 40 microns, the sharing would fall back to 22%. Of course the smaller pitch could also improve the resolution of Layer 00.

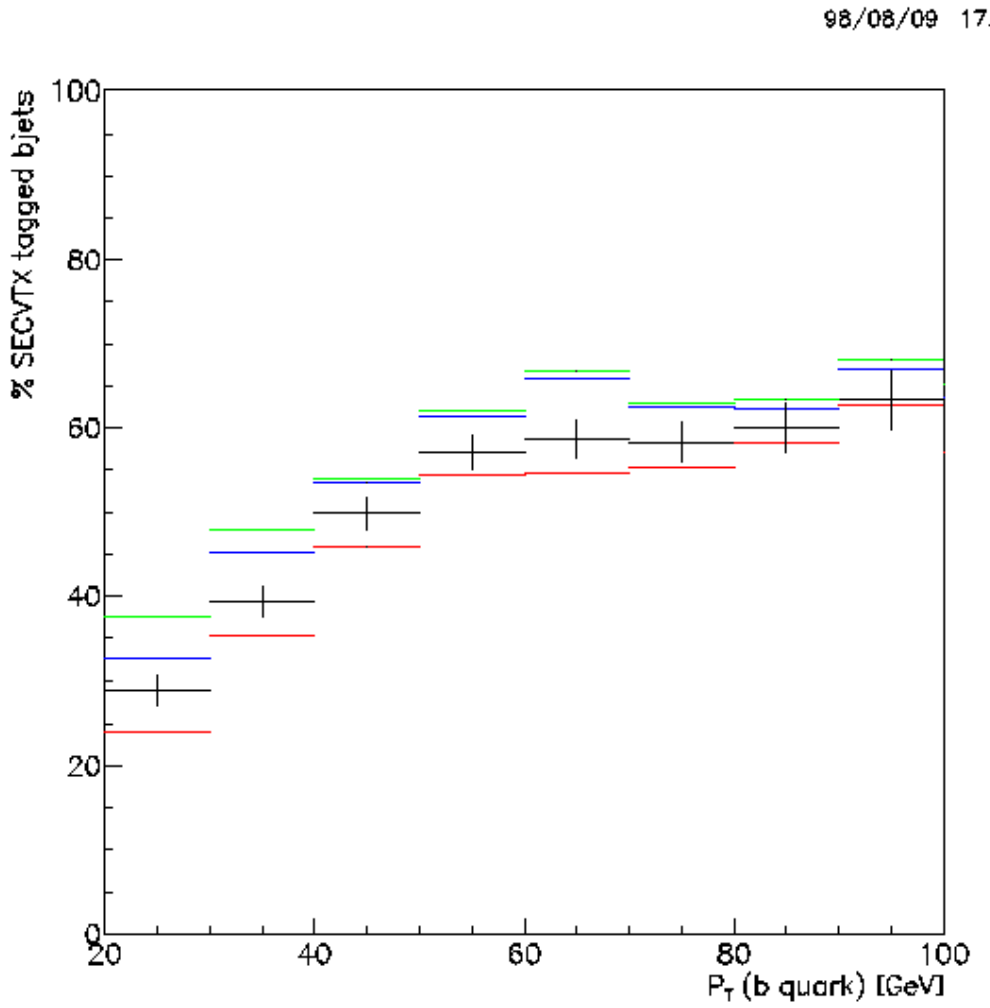

Figure 7: B tagging efficiency as a function of b quark P_T as discussed in the text.

- **Tagging as a Function of b quark p_T**

In this final section we include several plots demonstrating how Layer 00 improves b tagging as a function of p_T of the b quark. Figure 7 shows relative SECVTX tag rates versus the p_T of the b quark. The black crosses represent the results for SVXII. The vertical bars represent the statistical error. Since the same generated events are used in all of the calculations, the error bars are not repeated for the other plots. The blue entries (just above the SVXII case) are for SVXII with Layer 00. The highest entries (green) are for SVXII with Layer 00 and lower track p_T cuts (corresponding to equivalent resolutions). The lowest (red) entries are for SVXII after the demise of Layer 0. We see that for the case of standard SECVTX cuts, Layer 00 gives a relatively constant absolute increase in tag rates at all p_T. Of course the relative increase is larger at low p_T when one lowers the tracking thresholds (as seen in the highest entries).

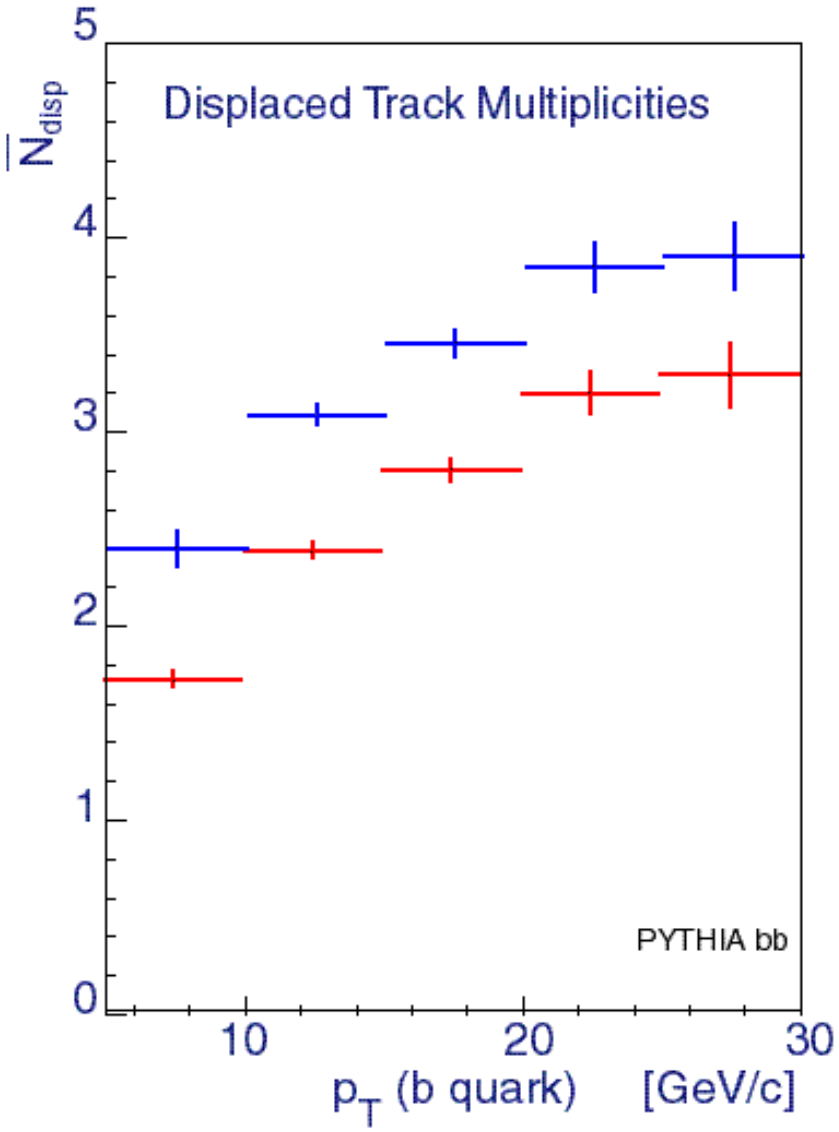

Figure 8: Mean number of detected displaced tracks in b jets as a function of b quark P_T as discussed in the text.

- **Low P_T Physics**

Using the machinery described in the last section, we generated b-bbar events. We then studied the effect of Layer 00 on multiplicity of displaced tracks as a function of the p_T of the b quark. Figure 8 shows the result of a comparison of significantly displaced tracks in SVXII alone (lower red entries) and SVXII with Layer 00 (higher blue entries) Note that these b's were selected by requiring at least one displaced track with $p_T > 2$ GeV. It is seen that Layer 00 increases the mean number of displaced tracks by more than 0.5 per b decay on average. This should improve our low p_T B measurements such as jet flavor tagging dilution. In run I, for instance, it was found that a SECVTX tag (with

broader jet definition) enhanced away-jet flavor tagging dilution by roughly a factor of 2. We have found that when using a jet cone radius of 1.0 and SECVTX track p_T cuts corresponding to equivalent track resolutions, the addition of Layer 00 results in a 98 % relative increase in the SECVTX single tag rate and a 289 % increase in the double tag rate. (Even with identical p_T cuts the latter shows a 55% increase.)

2.4 New Possibilities

Layer 00 could improve jet - parton associations as follows:

a) Displaced track multiplicity which is enhanced by the ability to reliably include tracks with momentum below 500 MeV/c. We find that the number of well-measured, significantly displaced tracks in b jets increases by ~0.5 on average at all b parton p_T up to ~40 GeV. At higher p_T the enhancement is smaller.

b) Detection of a tertiary vertex via reconstruction of two displaced vertices or the failure of the single vertex hypothesis.

c) Use of highly resolved primary and secondary vertex positions to define the b flight direction as an axis to be used for calculating a transverse mass. The shape of the distribution of this variable for many tags could conceivably be used to determine the relative contributions of b and c tags.

With higher purity of tracking, and better IP resolution, one can also detect secondary vertices nearer the primary vertex. The latter will lead to an improvement not only in b tagging, but also for tagging charm and possibly τ decays. This could be useful in a variety of particle searches. It would also help refine top studies.

3. Obstacles

The smallest practical radius for a silicon layer in CDF II is determined by the outer radius of the Beryllium beampipe at 1.51 cm.[***] Meanwhile, the innermost boundary of SVXII is at r = 2.10 cm. One problem already becomes clear: how to fit thousands of channels of silicon microstrips in a radial span of the order of an eighth of an inch, leaving another eighth inch clearance for installation inside SVXII? Even if you succeed, the radiation here is intense. The dose rate is double that of the inner radius of SVXII and we already worry about that layer. This is a problem that opens doors to still more problems. In particular, silicon exposed to such high doses of radiation must be kept quite cold - typically below 0 °C. This means that a cooling system must be interleaved with the silicon throughout the layer which further complicates the space problem. Also there are many reasons for requiring the innermost layer to be very lightweight. Achieving this, in turn, places added constraints not only on the cooling system, but on the mechanical support structure as well. The latter determines the stability and precision of the layer, which is needed to obtain precise hit position resolution.

[***] We have since learned that the beampipe o.d. could be reduced to as little as 1.1 cm.

An estimate of the radiation dose rate in CDF as a function of radius can be obtained using the measurement of 0.35 krad/ pb^{-1} obtained in Run I for the innermost layer of SVX′ together with the observed radial dependence of radiation at B0.[3,4] This yields

$$\Phi(r) = 2.22 \bullet r^{-1.68} \ \text{Mrad/fb}^{-1}$$

For a delivered luminosity of 3 fb^{-1} in Run II, this would predict an integrated dose on the innermost ladders in SVXII of 1.1 to 1.5 Mrad. Extrapolating, it follows that SVXII innermost layers will begin to experience thermal runaway and possibly cease to operate as a result of leakage currents induced by radiation damage at an integrated luminosity of ~ 3 to 4 fb^{-1}.[18] The inner layers will have to be replaced for Run III.[19]

The radiation situation is obviously worse for Layer 00. At 1.6 cm, the dose is double that of the innermost silicon in SVXII. We expect ~1.0 Mrad/fb^{-1}. This implies two serious problems. First, extremely rad-hard silicon must be used. We discuss the silicon in detail below. A second problem however is that this silicon must be kept cold and is itself a source of heat.

Averaging the rise in leakage currents as a function of integrated luminosity measured with the innermost layers of SVX and SVX′ in Run I, we obtain the following relationship.[4]

$$\delta I / \delta L = (0.50 \pm 0.14) \bullet (3.0 \text{ cm} / r)^{1.68} \ \text{nA / strip / pb}^{-1}$$

$$= 21 \bullet r^{-1.68} \ \mu\text{A / cm}^2 \text{ / fb}^{-1} \text{ (at 24 °C)}$$

At a radius of 1.6 cm, the corresponding value is 9.5 μA / cm^2 / fb^{-1}. As discussed below, the current is lower at lower temperatures. At 0°C for instance, it is ~ 1.3 μA / cm^2 / fb^{-1} while at it –10 °C becomes ~ 0.6 μA / cm^2 / fb^{-1}.

The silicon must be kept cold to limit reverse annealing.[11] The latter has the potential to ruin detectors in a matter of weeks. As will be discussed later, this effect can be slowed dramatically by maintaining the silicon at, or below 0 °C. It is a more serious problem for pixels where on-board electronics are distributed uniformly across the sensors. For microstrips, the electronics can be separated from the sensors. This was the case in the CDF SVX detectors and will be the case for the CDF ISL detector.[17] This does not eliminate the need to cool the sensors, but does dramatically reduce the amount of heat that needs to be removed from the active region. Another problem associated with pixels and other types of detectors with lots of on-board electronics is material.

While radiation, heat, material, and space are the most obvious problems that need to be dealt with, there are others. Some are technical. For instance, one needs to be sure beampipe currents and beam halo won't be a problem. Also, any motion of the beampipe must be minimized. Other problems are purely practical. These include manpower, engineering, time, and cost. We will address all of these issues.

4. Design

In this section we present a detailed design of a beampipe silicon layer. First we discuss the constraints which we feel are necessary to make the detector truly feasible. This is followed by an overview of two designs we have developed. Next we discuss the critical elements. The most critical of these is the rad-hard silicon. We therefore dedicate a significant amount of space to reviewing this topic. This is followed by signal cables and hybrids. The support structure and cooling system are then presented in detail, including results of calculations for heat removal, and thermal and pressure gradients. Next, we go over the material budget. The section concludes with a discussion of the data acquisition.

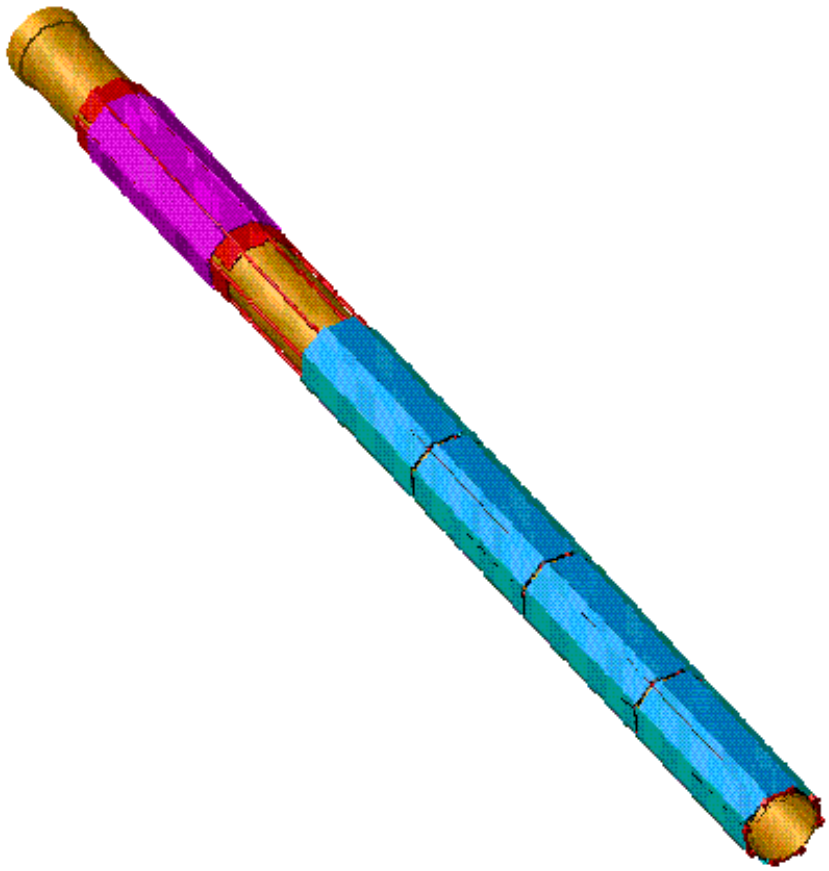

Figure 9. Solid model rendering of one half of Layer 00. Shown are 4 sensor groups (blue) starting at z = 0, and the hybrids (magenta) starting at z ~ 45 cm.

4.1 Constraints

In designing Layer 00, we have imposed a number of constraints. Some are fairly obvious while others may appear arbitrary. The latter were generally chosen to minimize the impact on existing upgrade work. Table 5 shows the main constraints that we considered.

The first item is the maximum radius of critical components. We chose the value of 1.9 cm because the Run II beampipe has a maximum radial protrusion, (stainless steel end-flange) at roughly this radius. We felt that by keeping all rigid components of the layer such as the substructure, cooling, and silicon itself below this radius, we would not seriously complicate the installation inside SVXII. The second item is our goal for radiation resistance. We chose a minimum lifetime dose of 5 Mrad. This will be seen to be conservative for the silicon, but is about where the SVX 3 chips have problems.[20] Importantly, this is roughly the amount of radiation the layer would receive if we were to double the integrated luminosity of Run II. This is the minimum one might do in order to further investigate an emerging signal for example. In regard to material, a 300 μm layer of silicon is itself roughly 0.3 % of a radiation length. Our goal is to add no more than about 0.3 % radiation length beyond this for most (80-90%) of the coverage of the layer. In the remaining regions where cooling services would be positioned, we intend to keep the total added material to ~ 1.0 %.

Table 5. Basic Design Constraints

Item	Constraint(s)
Maximum Radius of Critical Components	$R_{max} \leq 1.9$ cm
Radiation Tolerance (S/N ≥ 85 % initial)	$\Phi \geq 5$ Mrad
Typical and Peak Material Budgets	X ~ 0.5 % and ~1.0 % X_o
Percentage of Layer w/Typical and Peak Mat'l	~ 90 % and ~ 10 %
Percentage of all Silicon Channels	$N_{oo} \leq$ 2.5 % N_{TOT}
Coolant, Coolant Temp. & Operating Temp.	H_2O/Glycol, -10 °C, ≤ 0 °C
Pressure Drop	$\Delta p \leq 5.5$ psi
Mechanical Tolerances[†††]	± 25 μm
Manpower (Technician FTE)	≤ 2
Total Cost	~ 500 k$

The next few items address the impact of Layer 00 on the existing silicon projects. It cannot be a burden for the DAQ or mechanical assembly of the tracker. The total channel count is naturally restricted to a very low percentage of the current system, and the readout modularity was chosen to minimize DAQ costs while also assuring that the readout time does not exceed that of SVXII. Furthermore, we would use the same coolant and coolant temperature as SVXII in order to operate within the same chiller system. (The added volume is small). The maximum pressure drop is also the same as that specified for SVXII.

Finally, the effort involved in construction and installation should not exceed one man-year of technical labor and costs should not exceed ~500 k$. In sections 4 and 5 we present the designs and the construction plans we have developed to meet the criteria listed in Table 5.

[†††] Mechanical tolerances are discussed in greater detail in sections 5 and 6 below.

4.2 Overview of the Design

Only single sided (axial) detectors would be used in the small available radial space. To meet criteria for space, cooling, and material it is also necessary to combine some cooling and support structure functions. Naturally we take advantage of the beampipe to provide the majority of the support. We plan to wrap the beampipe in carbon fiber and build our support and cooling layers on top of it. The base layer would have thermally conductive carbon fibers (in the rϕ direction), to efficiently carry heat from the

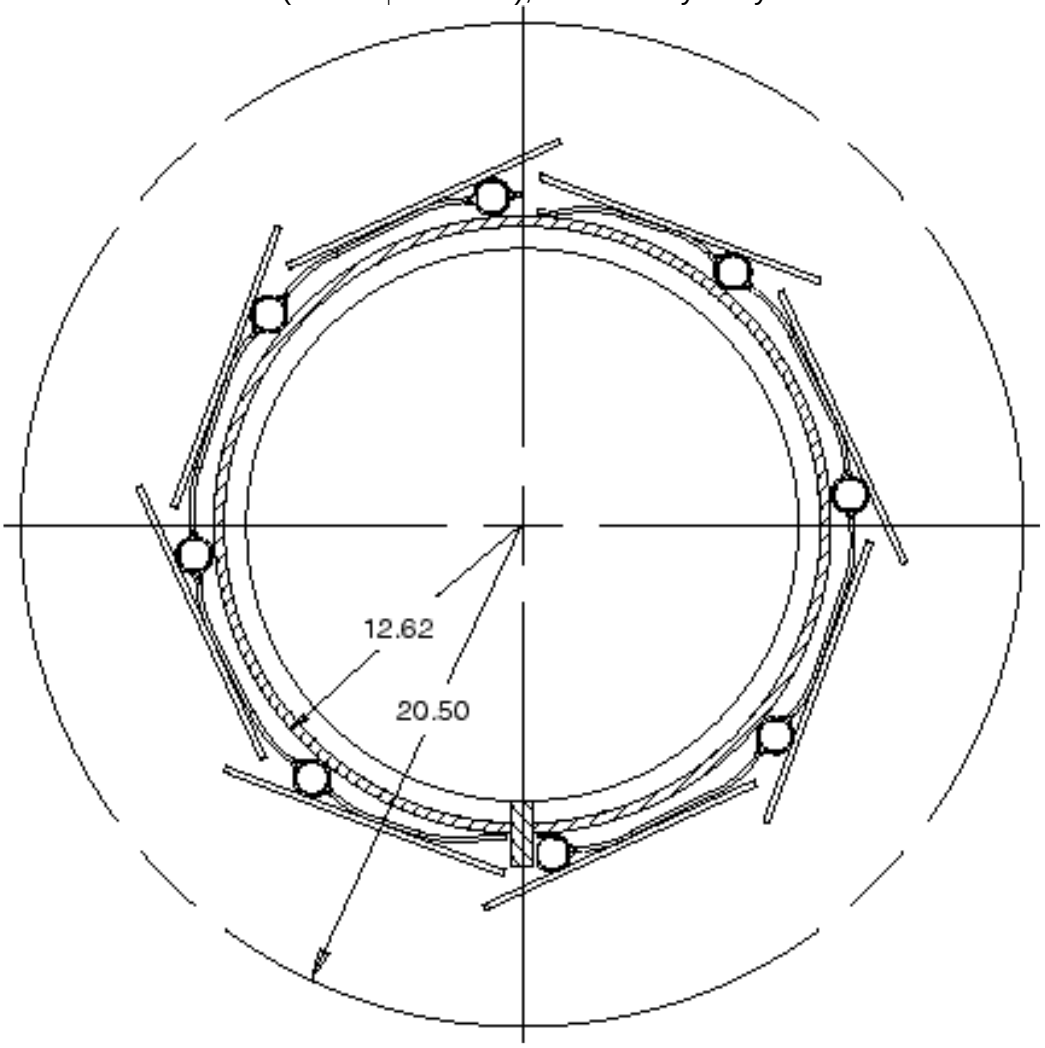

Figure 10. Layer 00 - Model A. Key features include the use of thin-walled metal cooling tubes trapped between plies of thermally conductive carbon fiber.

beampipe to the cooling channels. We plan to build Layer 00 in two pieces, (referred to as “clam shells” or “half cylinders”), each covering 180 degrees in azimuth. Initially we considered a design in which the silicon would be installed on a corrugated carbon fiber cylinder whose outside convolutions could act as sensor support ledges while the spaces between the base layer and the corrugated layer would be used to flow coolant.

Surprisingly this design resulted in almost two orders of magnitude more heat removal capacity than is necessary. It also caused us some concern to use carbon fiber as a fluid conduit. This led to designs in which small metal cooling tubes were interleaved with carbon fiber support layers. The current version of this line of approach will be referred to as model A, and is shown in a cross section view in Figure 10. A slightly different design, which eliminates the need for the carbon fiber supports, is shown in Figure 11 and will be referred to as model B.

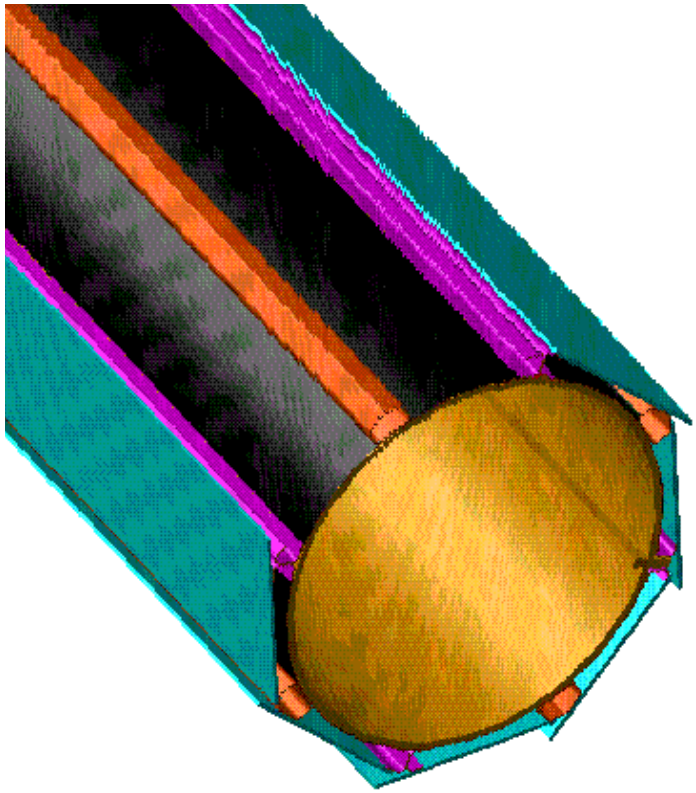

Figure 11. A slice through the model B design, with some silicon removed to show the cooling channel, intermediate support, and carbon fiber base ply.

Each of the models has particular advantages and disadvantages. Model A has the advantage of using simple cylindrical cooling tubes. The tubes are 1.5 mm inside diameter and have wall thickness of 50 μm if stainless steel is used, or 100 μm if aluminum alloy is used. Surrounding the cooling tubes is thermally conductive carbon fiber, which supports and cools the silicon layers. A very thin kapton layer insulates the back of the sensor from direct contact with the carbon fiber and also carries the bias voltages to the sensor back planes. This design provides excellent structural support and heat transport. The drawback is that the carbon fiber layers would need to conform to any irregularities in the surface of the beampipe. This would be achieved with a precise mandrill and very careful processing.

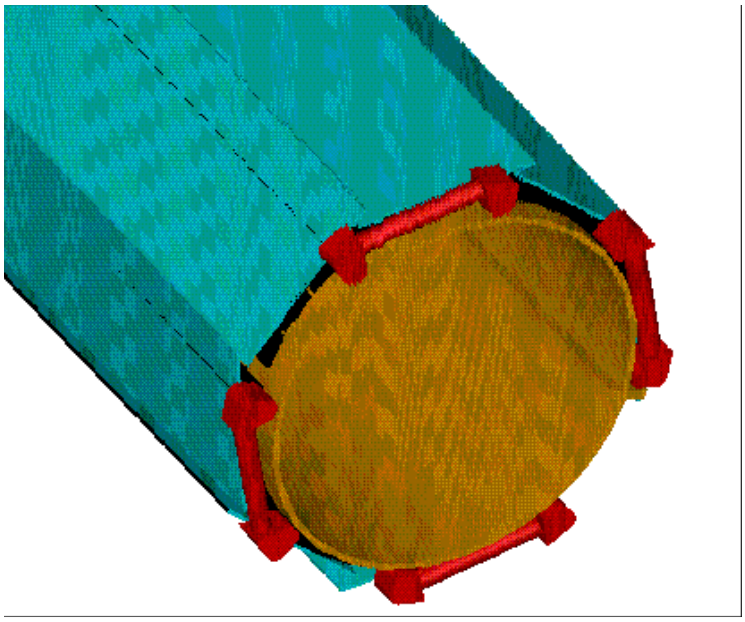

Figure 12. Cooling U-turns at z=0 using small cornering blocks and small sections of thin-walled tubing.

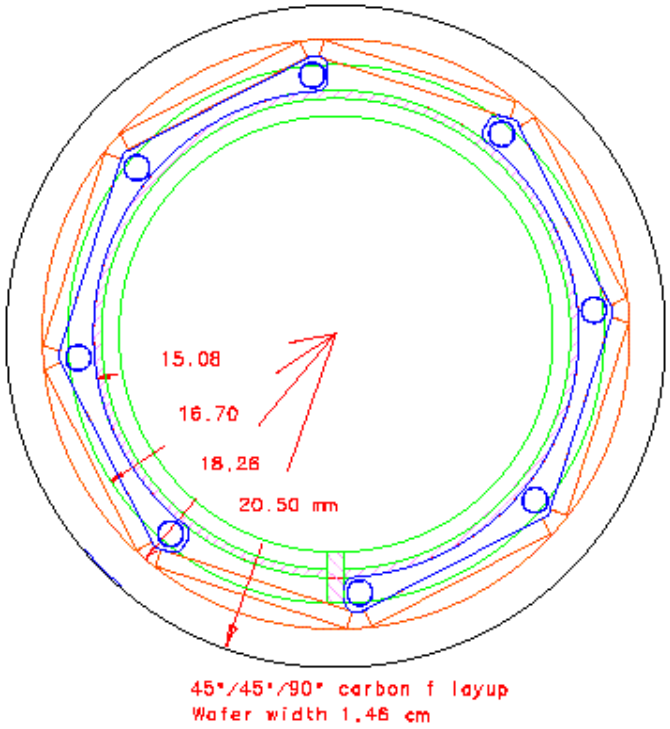

Figure 13. Cross sectional view of the hybrid cooling collar region. Each half cylinder has a collar (blue polygon sections) which supports and cools the readout hybrids (red rectangles).

Model B overcomes the problem of precision carbon fiber molding by using formed thin-wall cooling channels to act as support ledges. A thin kapton layer would again insulate the back of the silicon from direct contact with the cooling channel. By increasing the channel cross-section, the number can be reduced to two per half cylinder. Alternating with the cooling channels would be some simple supports. Carbon fiber I beams are shown in Figure 11 but these could be replaced with something simpler and less continuous such as small and precisely machined Beryllium blocks located at just 2 or 3 places per sensor. This would have the advantage of being easily tuned to irregularities in the beampipe by varying the height of the blocks. We originally thought that the need to form a precise cooling channel would be a serious drawback of this design. Using samples of thin-walled tubing however, we have found that it is relatively simple to form channels with polygonal cross-sections.

In both designs, coolant flows from outside to a cooling collar wrapped around the beampipe. The collar would allow some fluid to pass through to the cooling channels under the silicon layers. The flow route would do a U-turn at z = 0 as shown in Figure 12, then return to the initial distribution collar and back out to the chiller. A larger portion of the total flow would only circulate through the collar in order to cool the readout electronics installed directly on the collar, as seen in Figure 13.

4.3 Sensor Design[‡‡‡]

We intend to make use of recent R&D performed for LHC in the development of high breakdown voltage silicon sensors. Our sensors will be essentially equivalent to sensors designed for the CMS experiment.[7] These are expected to withstand an ionizing dose at the innermost barrel layer of ~10 Mrad. Sensors have now been consistently produced by a number of vendors that withstand test beam fluences of this level without more than ~10 % degradation in signal-to-noise ratio (S/N). In this section we will give a brief technical description of these sensors and also summarize our ongoing efforts for Layer 00 sensors.

4.3.1 Radiation Damage and Detector Specifications

Radiation damage can be classified as either surface or bulk damage in silicon. Surface damage is mostly manifested as holes trapped in either the oxide or oxide-silicon interface. The presence of these holes modifies the oxide field and leads to new energy levels in the forbidden energy gap. The deleterious effects are a decreased inter-strip isolation leading to unwanted sharing of charge between neighboring strips and increased inter-strip capacitance, which magnifies the noise. These effects can be countered by applying a bias voltage in excess of that needed for full depletion. The high, applied voltage forces free electrons, (which are attracted by the oxide space charge), into the gap between strips.

Bulk damage is due to the creation of lattice defects by radiation. These defects can act as electron-hole generation or recombination sites. In general, bulk damage leads to an increase ΔI in leakage current, which is linearly related to the integrated particle flux Φ by the expression:

[‡‡‡] This section is based upon the CMS tracking TDR discussion.[7] Alternatives include n+ on n and n on p detectors.

$$\Delta I = \alpha \Phi$$

The damage constant α depends on the type and energy spectrum of the radiation and also the temperature and biasing of the silicon. The dependence on temperature is found to take the form

$$I \propto T^2 e^{-E_a/kT}$$

Fits to data yield $E_a = 0.62 \pm 0.03$ eV. After allowing for detector annealing, the damage constant for 1 MeV neutrons at 20 °C is $(2.9 \pm 0.2) \times 10^{-17}$ A/cm and at -10 °C it is $(1.4 \pm 0.2) \times 10^{-18}$ A/cm. This implies a current density of 6 μA/cm^2 on the innermost layers of the CMS silicon barrels after 10 years of operation (T = -10 °C, and ~10 Mrad dose). For Layer 00 sensors operated at -5 °C, the active area is ~ 10 cm^2 and so the expected current per sensor after ~10 Mrad dose would be on the order of 100 μA.

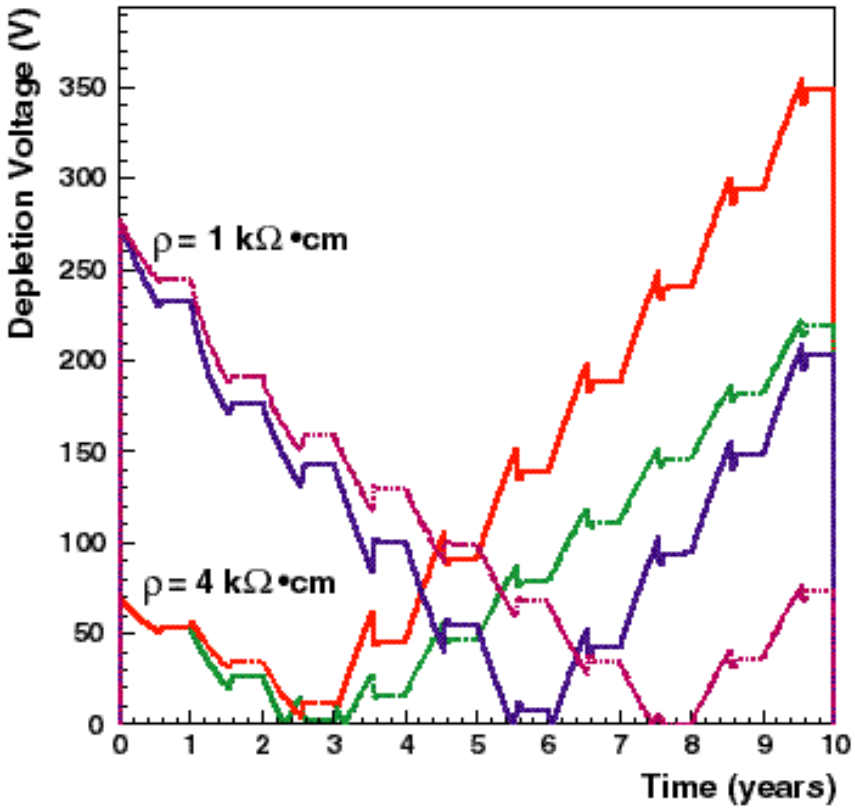

Figure 14. The expected evolution of the depletion voltage of CMS sensors with two values of initial resistivity and for radiation doses totaling 1.6 x 10^{14} n/cm^2 and 2.4 x 10^{14} n/cm^2 after 10 years.

Initially the sensor bulk is n-type as a result of a phosphorous (P) dopant, which creates donor sites. With irradiation the space charge, which was initially dominated by the P dopant, becomes increasingly negative. The absolute difference in P dopant donor site density and radiation induced acceptor site density is defined as the effective dopant concentration N_{eff}. With continued irradiation, the silicon becomes progressively less n

type and eventually inverts to become progressively more p type. The radiation flux Φ_{inv} leading to inversion scales with the initial resistivity (determined by the initial P dopant density N_o) of the silicon as $\Phi_{inv} = (18 \pm 0.6)\ N_o$. At inversion the acceptor and donor concentrations are balanced (N_{eff}=0). After inversion the acceptor sites dominate and N_{eff} can increase indefinitely. The evolution of the effective dopant concentration is important because it determines the depletion voltage of the device:

$$V_{dep} = N_{eff} \bullet (ed^2/2\varepsilon)$$

where d is the thickness of the sensor, ε is its dielectric constant, and e is a quantum of electric charge. It follows that the depletion voltage of the sensor should initially decrease with radiation to approximately 0 V at inversion, and then increase continually. For large radiation doses such as those anticipated at LHC, or by CDF at small radius, the depletion voltages of sensors is expected to rise dramatically. CMS has developed sensors with breakdown at bias voltages in excess of 500 V. The evolution of the depletion voltage for these sensors operated at the LHC over a period of 10 years with regular intervals of no beam is shown in Figure 14.

Annealing effects complicate the time evolution of N_{eff}. In addition to a stable component of radiation damage, there are unstable components that can either diminish or increase even after exposure has stopped. These are called beneficial and reverse annealing, respectively. The latter can be adequately slowed by operating below 0 °C but can seriously degrade sensors in a matter of weeks at room temperature. Reverse annealing does not become significant until the detector has gone through type inversion. As a result, detectors that have significant radiation doses must be kept at low temperature except for perhaps a few days per year.

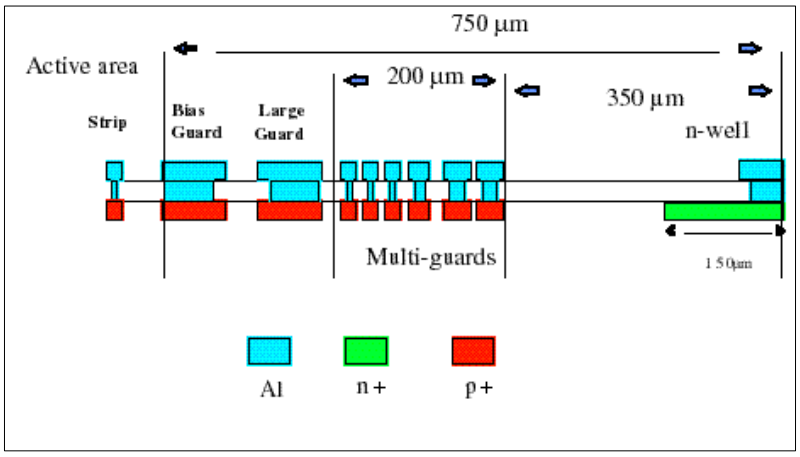

Figure 15. Schematic diagram of the CMS sensor guard ring structure.

The LHC research program has resulted in design and processing specifications for silicon sensors to allow the consistent production of high operating voltage sensors. We will briefly describe the salient features of these specifications, and then give a summary of results obtained for sensors manufactured accordingly, before and after irradiation.

The list of specifications is rather detailed but can be divided into design and processing categories. With regard to design, the most significant considerations are the

treatment of the edges of the sensors, the implant shapes, and the oxides for both the surface passivation and the coupling capacitors. The edge of the sensor is generally fraught with defects as a result of the cutting process and can easily result in breakdown across the bulk or act as a significant source of current. To counter these possibilities a n+ guard ring is placed on the top surface near the edge. Extending from 350 μm, to 550 μm from the edge is a multiple p+ guard structure. This assures that the electric fields on the surface do not have a large gradient. The overall surface structure is diagrammed in Figure 15. The leakage current per strip is required to be less than 0.5 μA at 500 volts of bias after irradiation, and less than 50 nA before irradiation.

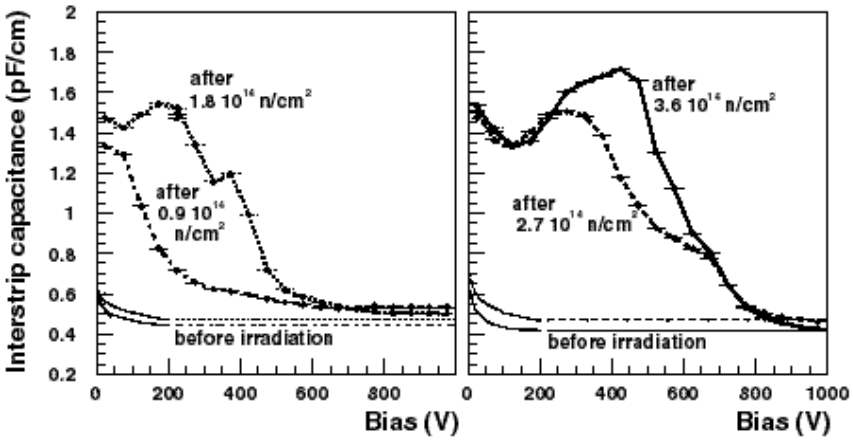

Figure 16. Interstrip capacitance vs. bias voltage.

4.3.2 Results with Prototypes

Irradiation leads to concentrations of positive fixed charge in the oxide layers, which eventually saturate. These lead to higher concentrations of charge at the interface of the oxide and the silicon which increases the inter-strip coupling. As seen in Figure 16, the effect can be reduced by an increase in bias voltage. High fields on the p^+ side confine the interface electron concentrations to small regions in the gap between strip implants. Detectors have been produced with adequately high biasing capabilities. Figure 17 shows a distribution of breakdown voltages for CSEM detectors. Figure 18 shows the stability of these sensors with operating conditions and with irradiation up to 10^{14} n/cm^2. Figure 19 shows I-V curves for full size Hamamatsu devices after intense proton and neutron irradiation.

Breakdown usually occurs in the proximity of the silicon surface close to the junction termination. Other sources of strong current increases include surface generated leakage and currents injected from the edge region. A biased guard ring around the active region collects surface currents while an n-well along the edge of the detector creates a barrier against hole injection.

High applied voltages can lead to possible avalanche breakdown on the external side of the guard ring causing detector noise and eventually physical breakdown of the device. To avoid this, the external field is controlled by a multiple guard ring structure as discussed above. It has been determined in prototype studies that the separation

between the n well and outermost p+ ring must be at least 150 μm for optimum breakdown protection.

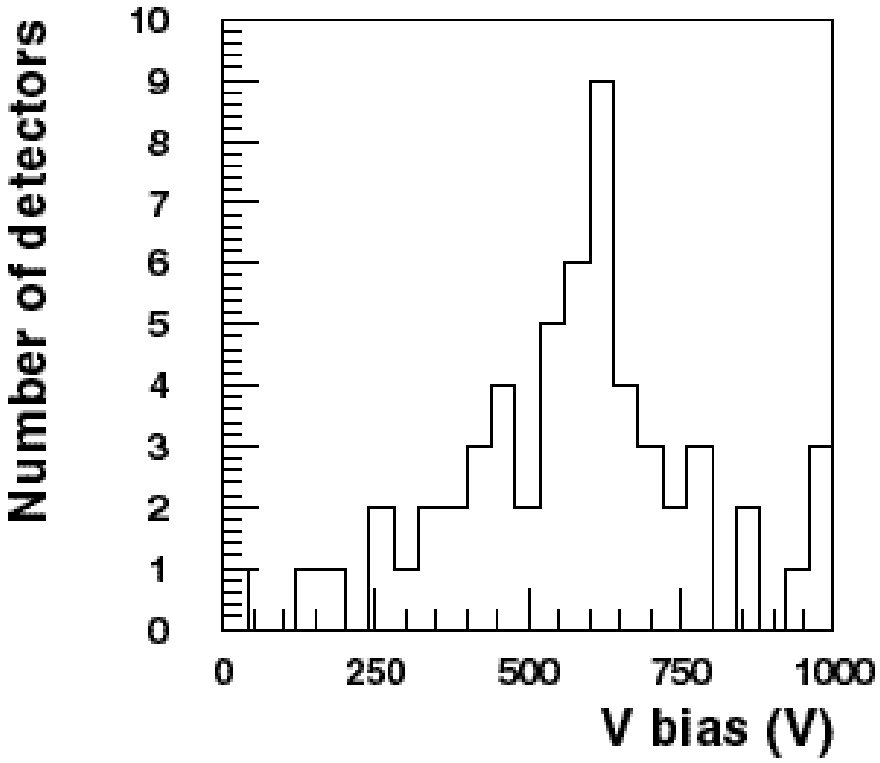

Figure 17. Breakdown voltages for full size detectors produced by CSEM. The average is 580 V with rms spread of 200 V.

4.3.3 Test Beam Results

The Signal to Noise ratio (S/N), hit efficiency, resolution, temperature and irradiation performance of high bias voltage detectors was studied in various test beams. With regard to S/N the relevant parameters are pitch (p), and width (w) and length (l) of the implant. In fact, for a given bias voltage, the S/N is relatively constant for fixed ratio of p/w. For a length of 12.5 cm, the S/N was found to be roughly 25 at room temperature and improved some 20% in going to -10 °C.

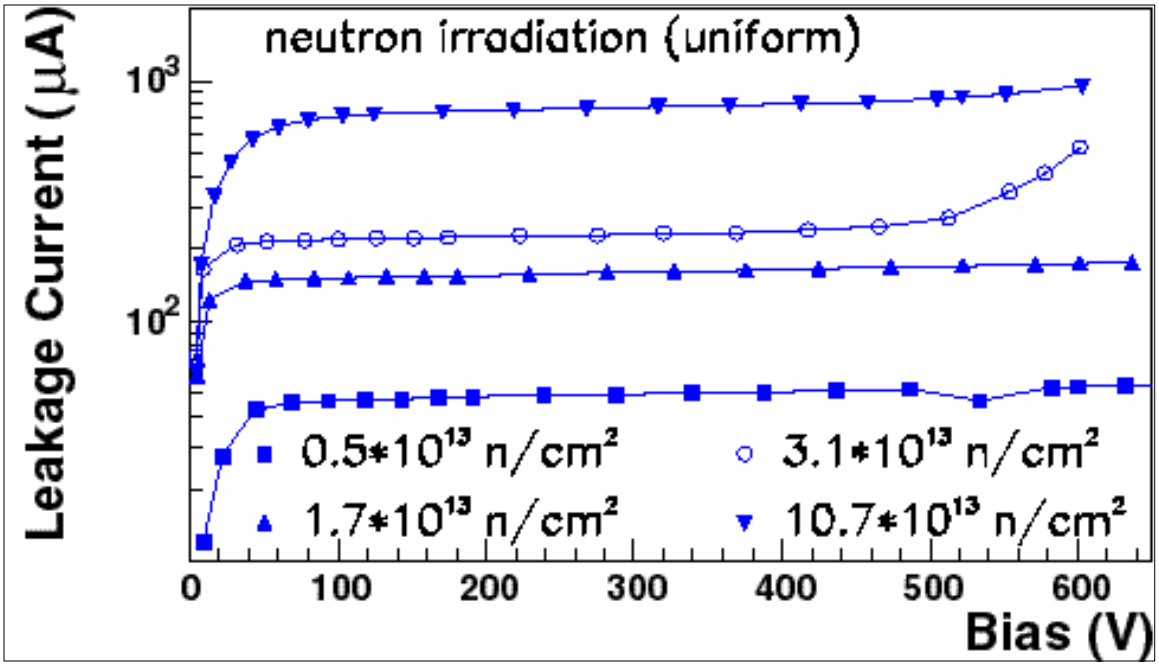

Figure 18. Current versus voltage: breakdown behavior of a CSEM sensor.

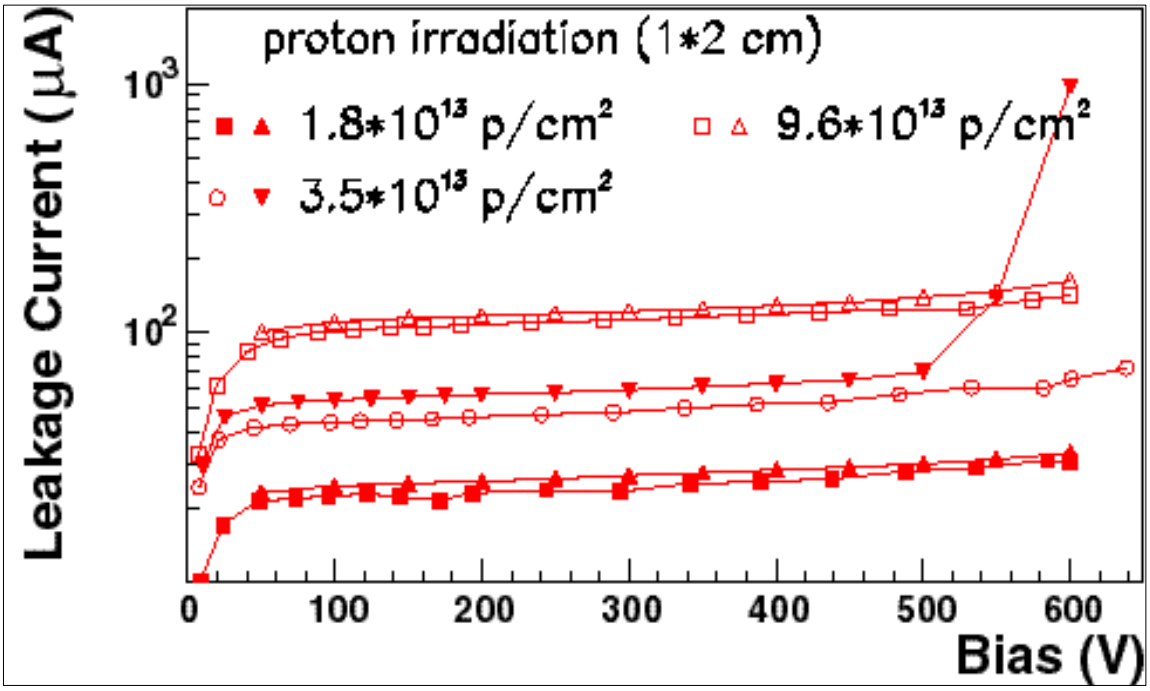

Figure 19. I-V curves for full size Hamamatsu sensors after p and n irradiation.

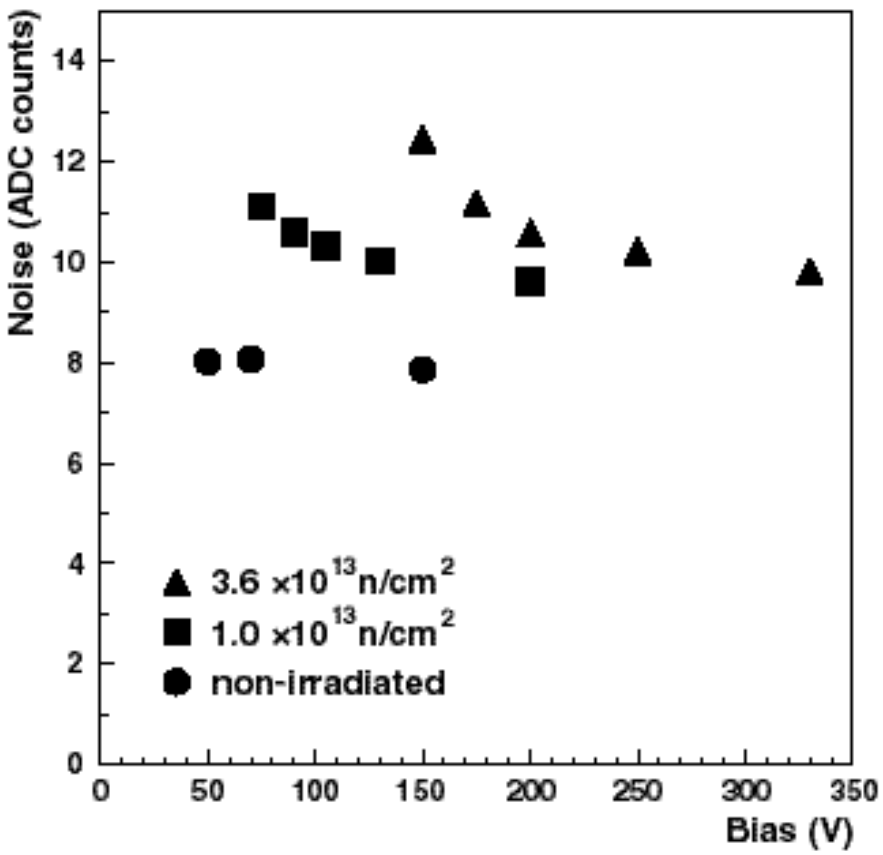

Figure 20. Noise as a function of bias voltage.

The effect of irradiation is to increase noise as a result of increased inter-strip coupling as seen in Figure 16 and to decrease charge collection efficiency as a result of bulk damage. These effects are diminished by an increase in bias voltage as shown in Figure 20. Figure 21 shows that not more than ~10 % of S/N is lost for a dose of 10^{14} n/cm^2. The S/N approaches a plateau for high voltage as seen in Figure 22. Figure 23 shows results for CSEM sensors, similar in design to what would be used in Layer 00, after doses up to ~ 3.6 x10^{14} n/cm^2. One sees a similar behavior in S/N versus overdepletion factor independent of fluence.

CMS has included prototype Layer 00 detectors on masks, which will be used to make sensors in 1998. The designs for the Layer 00 sensors which are 50 μm readout pitch and both with and without intermediate strips can be viewed at: http://wwwcdf.pd.infn.it/cdf/sildet/cdf_l00_masks.html

4.4 Lightweight Cables

As mentioned above, the ability to place the readout hybrids outside the central tracking region is critically important for cooling and space, and also improves the performance. The cables we plan to use are kapton, with a total thickness of 50 μm. The traces on such cables can be made roughly 20 μm wide with 50 μm pitch. Currently

these cables are made at CERN[21] and elsewhere in Europe and the US. The traces are 5 μm thick copper, with 200 Angstroms of Nickel. The cables represent only 0.023 % of a radiation length.

With 50 μm pitch, the cables have a capacitance 0.46 pf/cm to be compared with ~1.0 (1.4) pf/cm for the silicon detectors with 50 (25) μm pitch. Since the cable lengths for the sensors nearest z = 0 are quite long, the added capacitance becomes significant in increasing noise. To overcome this, we plan to use two 100 μm pitch cables for the longest paths. The capacitance per unit length is then halved and the maximum added capacitance is roughly 8 pf resulting in a total capacitance of less than ~22 pf. This will result in excellent S/N.

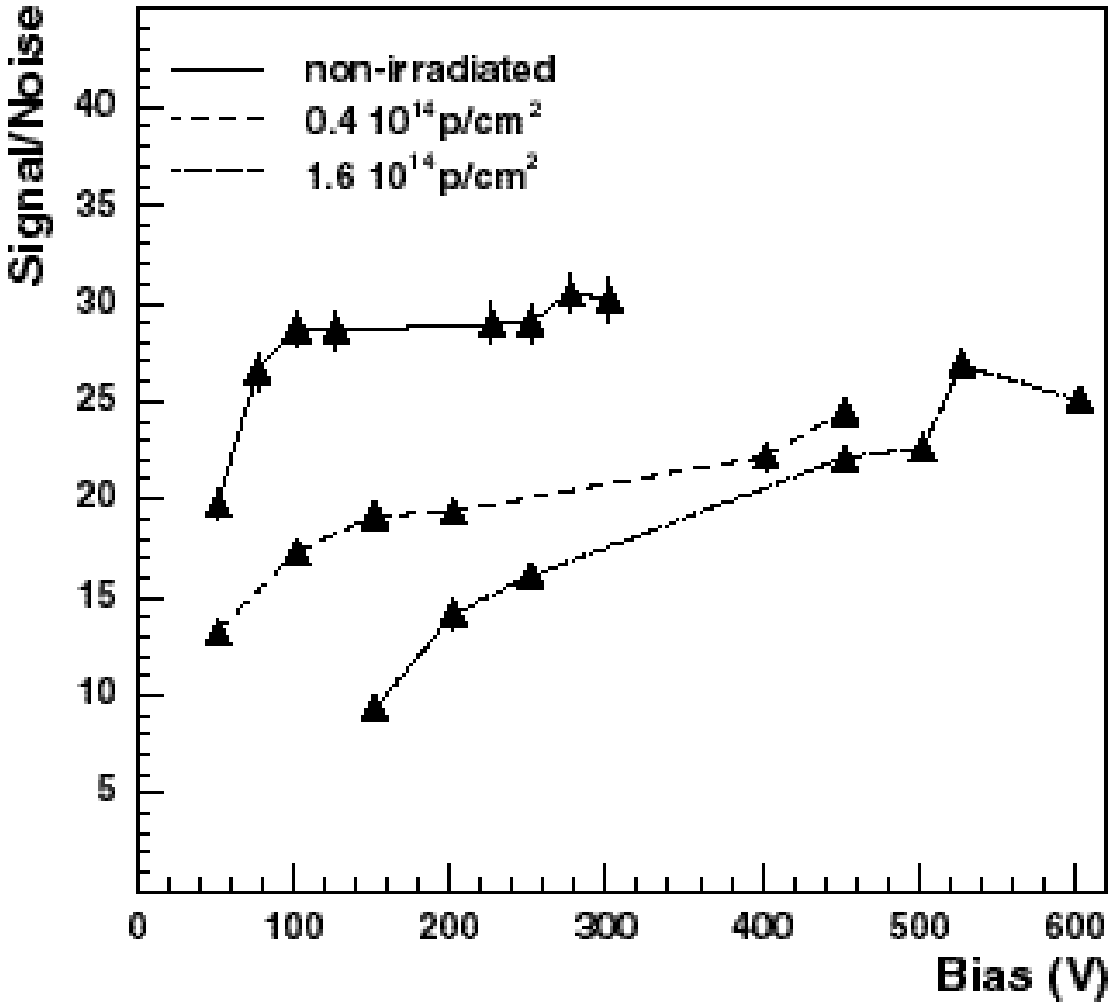

Figure 21. Collected signal as a function of bias voltage for Hamamatsu proton irradiated devices with 6.25 cm strips and 80 μm pitch.

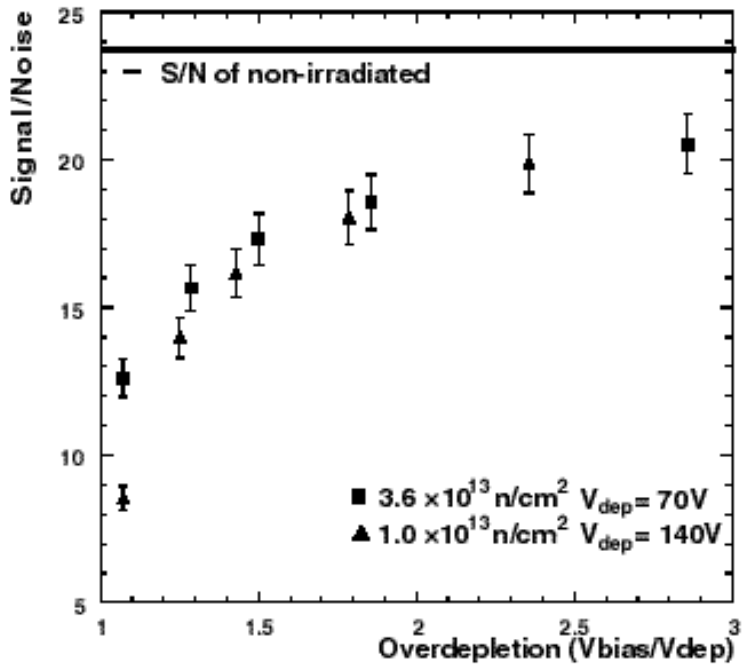

Figure 22. S/N versus overdepletion factor for SINTEF sensors.

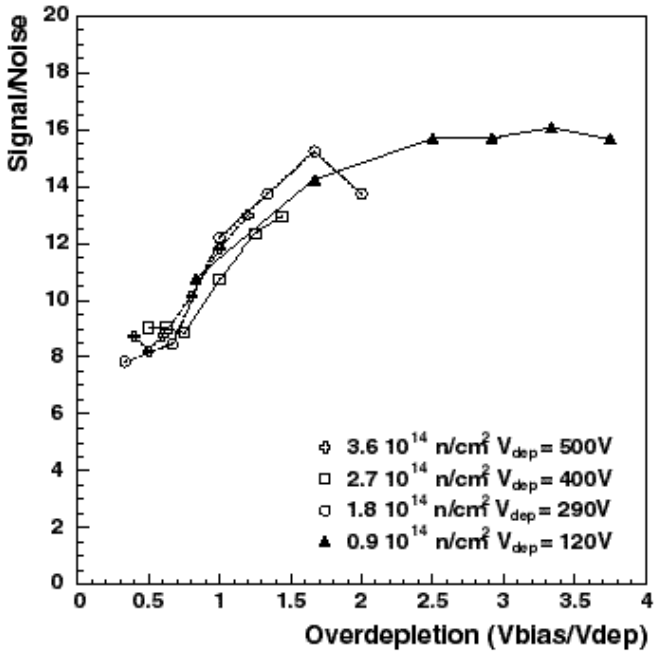

Figure 23. S/N for heavily irradiated CSEM sensors with 50 μm pitch and 12.5 cm length that is very similar to what would be used for Layer 00.

4.5 Hybrids

The hybrids are expected to be fairly straightforward adaptations of the ISL hybrids. They will be manufactured on Aluminum Nitride, which can be as thin as possible since the hybrid is single sided and will lie directly on top of a cooling collar. The hybrids are restricted to be somewhat narrow (~ 1.25 cm) but can be fairly long. One possibility is to make a hybrid that handles two chips staggered in z. Four such hybrids would be stationed at the end of a row of 4 sensors. The material associated with the hybrids and cooling collar can be kept fairly low since the hybrid is single sided. Nevertheless, this region will have more material than the central region.

4.6 Support Structure

We will use the beampipe as the main support structure in order to minimize the material required. The beampipe will be surrounded by a single ply of thermally conductive carbon fiber. This will act as a base to which the cooling tubes (with or without carbon fiber sleeves) and support staves can be glued.

We have estimated the total mass of Layer 00, including coolant, to be ~ 200 grams. Prior to installing the layer, the beampipe sag, when supported at the end of the ISL spaceframe and the COT face, has been calculated[22] to be 0.001" for the case of supports at ±1.5 m. With the addition of Layer 00, the sag becomes 0.007". This is quite small, and will allow fair separation from SVXII.

4.7 Cooling

In this section we cover the performance of the cooling system which relies on very small, long cooling channels. We first discuss heat sources. We then show by calculation and test that we can get adequate cooling with small diameter tubes as proposed for model A. The channels used in model B are more than a factor of two larger in cross-sectional area than the tubes used in the study. Since the pressure gradients vary roughly as the square of the cross-sectional channel area, it follows that model B will also have more than adequate cooling even with a factor two fewer cooling channels. We go on to determine the expected temperature of the sensors after extreme radiation exposure.

4.7.1 Heat Sources

The SVX3 front-end readout chips consume roughly 0.5 W each and the layer would contain 64 of them on each end. This is the dominant source of heat but not a serious concern. The large surface area of contact between the hybrids and the cooling collars, together with the relatively high flow rate of coolant through the collar, will provide ample heat removal.

The largest source of heat for the sensors is the ambient environment. We define the Layer 00 volume to be the space between the Layer 00 silicon at radius r_0 = 1.6 cm and the inner screen of the SVXII detector at radius r_s = 2.1 cm. For simplicity, assume this volume, as well as the space between the inner screen and the innermost layer of SVXII, is filled with dry Nitrogen gas having little or no forced flow. Next assume that layer 0 of SVXII is at radius r_0 = 2.5 cm and at temperature T_0 while Layer 00 is at temperature T_{00}.

The current expectation is for T_0 = 15 °C. We will also consider the conservative value T_0 = 25 °C and take T_{00} = -10 °C. A schematic cross section of the system being modeled is shown in Figure 24.

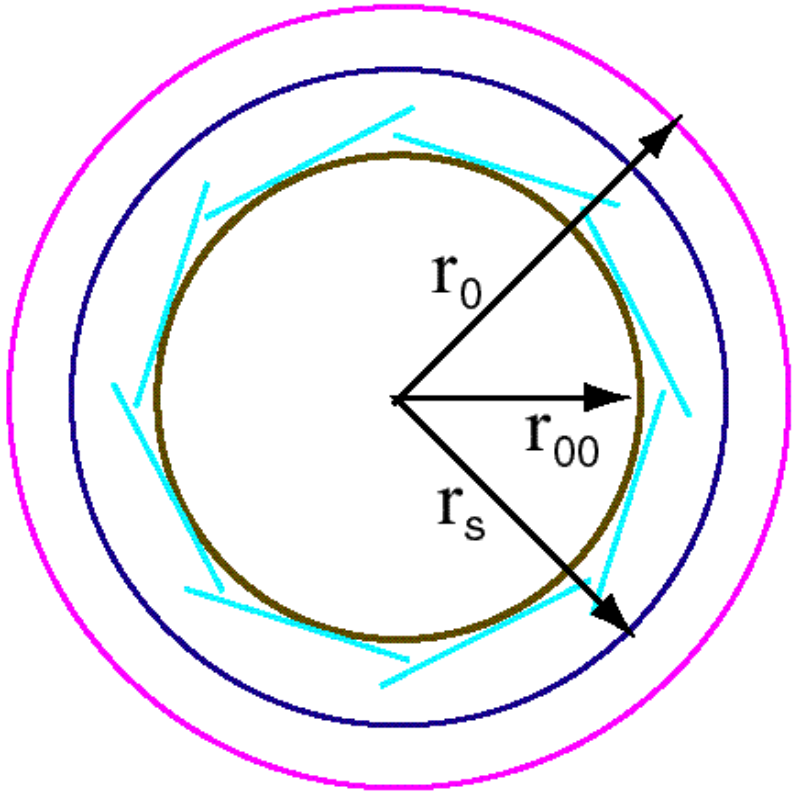

Figure 24. Model used to calculate heat transfer from the ambient environment.

The convective heat transfer between two concentric, infinitely long cylinders, (with $r_n > r_m$) is given by the expression.[24]

$$q_{mn} = 2\pi\, k_{eff}\,(T_n - T_m)/\ln(r_n/r_m)$$

where k_{eff} is the effective thermal conductivity of the gas, including free convection. The radiative heat transfer for this geometry is given by the expression

$$Q_{mn} = \sigma \bullet (T_n^4 - T_m^4)/[(1/\varepsilon_m) + (1-\varepsilon_n) \bullet (1/\varepsilon_n) \bullet (r_m/r_n)]$$

Where the ε's are the emissivities of the surfaces and σ is the Stefan-Boltzmann constant. For our case, the equilibrium condition corresponds to the situation in which the heat transfer from SVXII layer 0 to the inner screen equals the heat transfer from the inner screen to Layer 00. This can be expressed symbolically as $q_{0s} + Q_{0s} = q_{s00} + Q_{s00}$. The equilibrium condition allows one to solve for T_s, the temperature of the inner screen, and for the net heat transfer to Layer 00. For the effective thermal conductivity of the gas we use $k_{eff} = \alpha\, k$, where k is the standard thermal conductivity and $\alpha \geq 1$ is a factor that takes into account the increase in thermal conductivity resulting from free convection. The constant α is difficult to calculate. For similar temperatures and geometries,

examples found in the literature indicate a value less than 1.5. We used the range $1 \leq \alpha \leq 2$ for four different cases as shown in Figure 25. We made the conservative assumption that the emissivity of silicon is $\varepsilon = 1$. The cases in the figure correspond to $T_0 = 15$ and $\varepsilon_s = 1$ or 0.05. The value $\varepsilon_s = 1$ is what would be expected for a simple carbon fiber screen. The lower value of 0.05 can be obtained by laminating the carbon fiber surfaces with ultra-thin Aluminum foil. In the latter case, the heat transfer per meter length, even in the extreme case of $k_{eff} = 2$ k, is on the order of 15 W. This corresponds to 12 W for all of Layer 00. Recently we have measured α directly with a mock-up of the system and find $\alpha < 1.10$. We conservatively estimate the ambient heat load on Layer 00 to be below 15 W (where we assume little or no reduction in thermal radiation.)

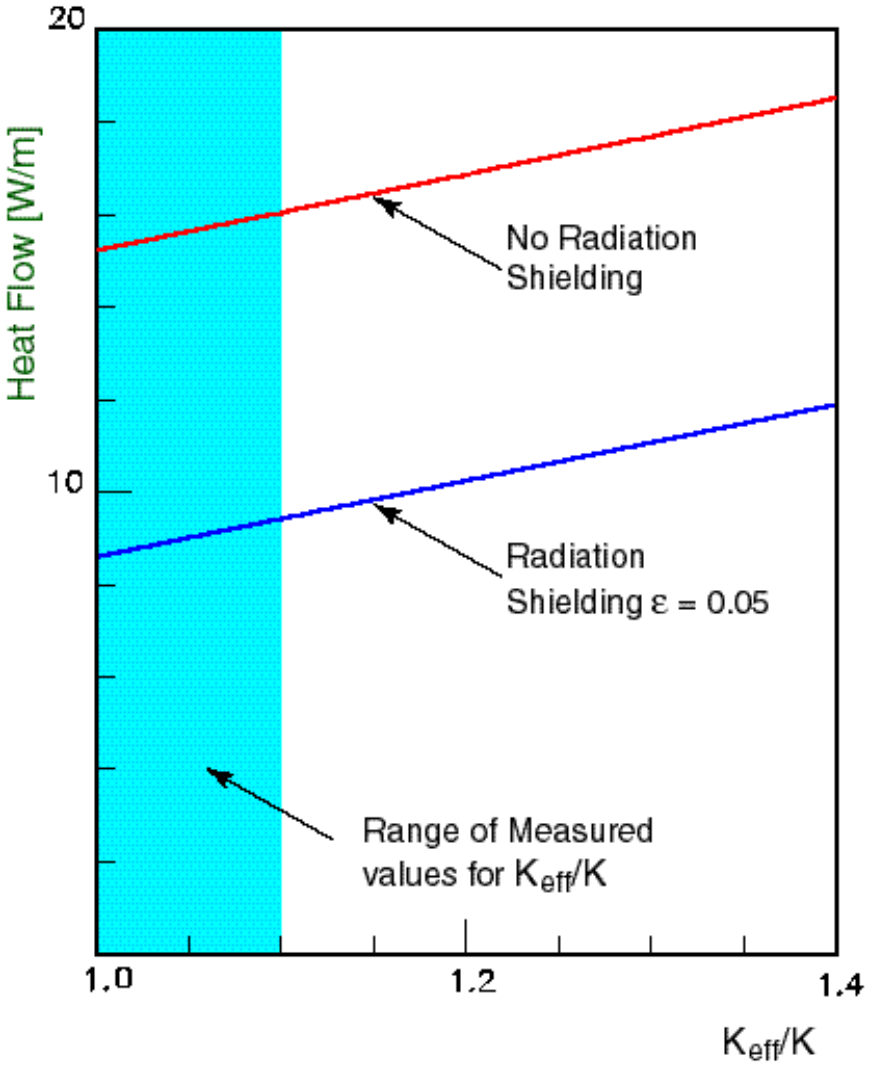

Figure 25. Ambient heat flow to Layer 00 as a function of $\alpha = K_{eff}/K$. The curves are for $T_0 = 15$ °C and inner screen emissivity $\varepsilon = 1$ (top) or 0.05 (bottom). The vertical band shows the region of measured values of $\alpha = K_{eff}/K$.

Radiation damage is expected to result in an increase in leakage currents of ~1.3 $\mu A/cm^2/fb^{-1}$ at the radius of Layer 00 for an operating temperature of ~0 °C. The heat dissipation per unit area after 10 fb^{-1}, under the assumption that the operating voltage for the radiation-damaged sensors is 500 V, is then 6.5 mW/cm^2. The surface area of the entire layer is ~ 1000 cm^2. The power dissipated by Layer 00 is thus 6.5 W.

Image currents of the proton and antiproton beams in the Be beampipe could also be a source of heat. In Run II the Tevatron will have up to 108 bunches of 2.4×10^{11} protons and an equal number of bunches with 1.0×10^{11} antiprotons. The bunch spacing is 132 ns and the bunch length is roughly 0.2 m. A calculation determines that the power dissipated per unit length of beampipe by image currents is 0.2 W/m. Following more careful calculation procedures used by the Fermilab Accelerator division[23] we obtain the range 0.15 to 0.33 W/m.

From the above discussions, we thus conservatively estimate the maximum heat transfer to Layer 00 as $Q \leq (12 + 6.5 + 0.5)$ W = 19 W. For the model A (B) design there are a total of 8 (4) cooling circuits. Each circuit would need to be able to remove ~2.4 (4.8) W of heat *after a radiation dose of ~ 10 Mrad*.

As an aside, note that the beam currents could also be a source of noise. Although Beryllium is not a great conductor, for the frequencies associated with the beam currents, the skin depth is of order 32 μm. The beampipe itself has wall thickness of 508 μm. This should be adequate to shield Layer 00. A more serious concern is that the beampipe outer surface could act as an antenna. We would protect against this by placing a very thin, isolated layer of Aluminum under Layer 00 that would be connected to a quiet ground. This would add as little as 0.06 % X_o of material.

Ionizing particles also generate heat in the beampipe. Based on the expected flux of $F = 2.2 \times r^{-1.68}$ $Mrad/fb^{-1}$ and an instantaneous luminosity of 2×10^{32} $cm^{-2}\,s^{-1}$, we estimate an average of 0.2 mW/m of heat from radiation. This rises to ~ 6 mW/m for radiation at the level required to abort the beam (2 rad/sec at 3 cm radius).

4.7.2 Pressure and Temperature Gradients in Very Small Channels

We now calculate the heat removal ability of Layer 00 cooling system designs. Heat absorbed by a fluid in a cooling channel is given by the expression:[24]

$$Q = \pi\, h\, d\, L\, \Delta T$$

where Q is the heat load [Watts], h is the convection coefficient [W/°C -m^2], d is the inside diameter of the tube [m], L is the heated length [m], and ΔT is the difference between the inner wall surface and bulk coolant temperatures. The expression for the convection coefficient h is:

$$h = Nu\, k / d$$

where Nu is the Nusselt number, a dimensionless characteristic of the convective heat transfer performance and k is the thermal conductivity of the coolant [W/°C - m].

In general, Nu varies with the cooling channel geometry, fluid flow rate, and other fluid properties. However, for fully developed laminar flow with a constant, uniform heat flux, Nu is a constant, with a value of 4.36 for a circular channel cross section. Substituting this into the energy balance equation above yields $Q = \pi \, Nu \, k \, L \, \Delta T$ which is independent of d.[§§§]

We calculated the radial temperature gradient of the fluid for a mixture of water and ethylene glycol (30 % by weight[****]) at an inlet temperature of -10 °C. The cooling tube was assumed to consist of two, straight sections, each 50 cm long and connected at one end to form a U-shaped route. It was also assumed that heat is dissipated uniformly along the length of the tube. Parametric studies were performed in which the following three quantities were varied: a) Tube diameter d = 1, 1.25, and 1.5 mm b) Total Heat Load Q = 0.4, 1.2, and 2.0 Watts and c) Flow rates to yield 1.0, 1.5, and 2.0 °C inlet-to-outlet coolant temperature rise

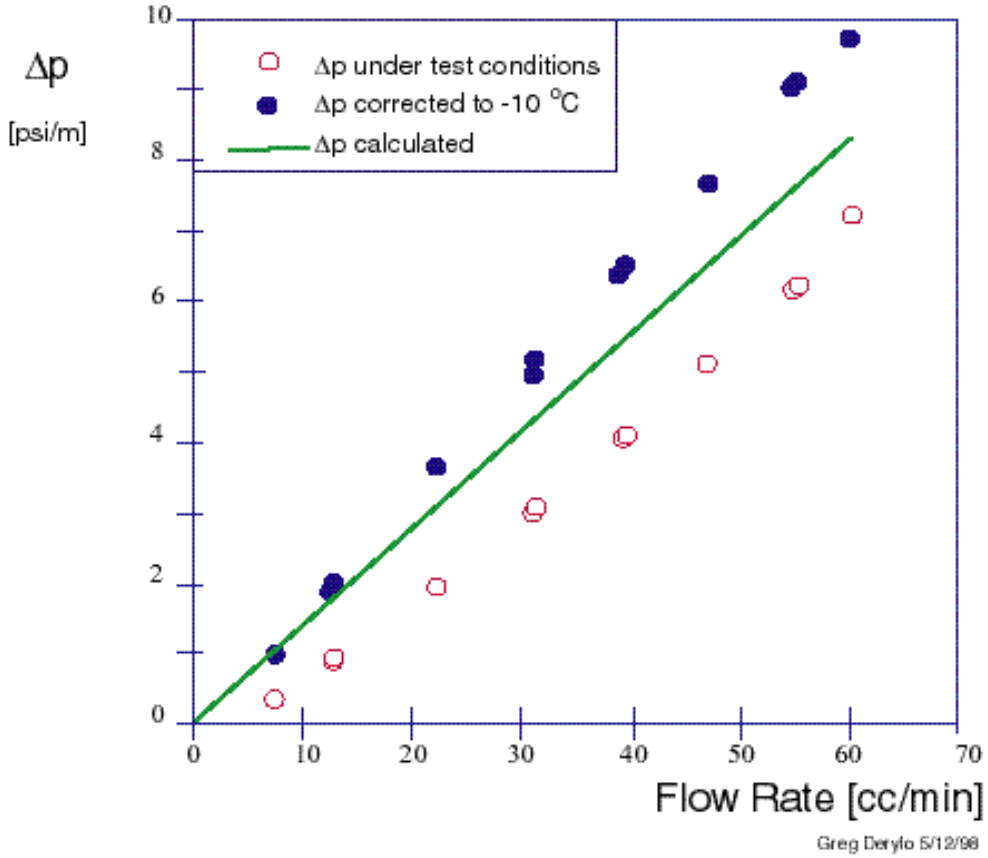

Figure 26. Measurement of pressure drop in a cooling tube similar to that for model A. Open circles represent actual data, solid circles are the result of correcting the viscosity to - 10 degrees. The line shows the result of the calculation.

For the various possible combinations of these values, we determined the fluid flow rate [liters/min], velocity [m/s], pressure change [psi] and Reynolds number. He also

[§§§] Pressure drop, however, is a strong function of the channel diameter d.
[****] As currently planned for SVXII.

determined the convection coefficient [W/°C -m^2] and temperature gradient ΔT. The results are presented in Table 6.

One sees that it is possible to have a reasonable pressure drop of 5.6 psi and a very small radial temperature rise $\Delta T \cong 0.21$ °C when the temperature rise in the fluid is allowed to be 2 °C (inlet-to-outlet). This is what is expected for a 1.2 W load and a 1 mm tube diameter. For a 1.5 mm diameter tube, as envisioned for Model A, we can extrapolated to 5 W, which is double the maximum expected heat load. There is still no real difficulty. The pressure change and radial temperature gradient of the fluid in the tube are 5.5 psi and 0.34 C for an inlet-to-outlet temperature difference of 2 C. Channels to be used for Model B would have roughly twice the cross sectional area so that the same heat load could be handled with half as many conduits.

Table 6. Calculation Results for a Circular Cooling Channel

ΔT in-to-out [°C]	D [mm]	Q [W]	flow rate [liters/s]	Velocity [m/s]	Reynolds Number	Δp [psi]	$\langle h \rangle$ [W/°C-m^2]	ΔT thru fluid [°C]
1.0	1.00	0.4	0.006	0.13	24	3.9	1850	0.07
1.0	1.00	1.2	0.019	0.40	71	11.6	1850	0.21
1.0	1.00	2.0	0.032	0.67	118	19.4	1850	0.34
1.0	1.25	0.4	0.006	0.09	19	1.6	1480	0.07
1.0	1.25	1.2	0.019	0.26	57	4.8	1480	0.21
1.0	1.25	2.0	0.032	0.43	94	8.0	1480	0.34
1.0	1.50	0.4	0.006	0.06	16	0.8	1230	0.07
1.0	1.50	1.2	0.019	0.18	47	2.3	1230	0.21
1.0	1.50	2.0	0.032	0.30	79	3.8	1230	0.34
1.5	1.00	0.4	0.004	0.09	16	2.5	1850	0.07
1.5	1.00	1.2	0.013	0.27	48	7.6	1850	0.21
1.5	1.00	2.0	0.021	0.45	80	12.7	1850	0.34
1.5	1.25	0.4	0.004	0.06	13	1.0	1480	0.07
1.5	1.25	1.2	0.013	0.17	38	3.1	1480	0.21
1.5	1.25	2.0	0.021	0.29	64	5.2	1480	0.34
1.5	1.50	0.4	0.004	0.04	11	0.5	1230	0.07
1.5	1.50	1.2	0.012	0.12	32	1.5	1230	0.21
1.5	1.50	2.0	0.021	0.20	53	2.5	1230	0.34
2.0	1.00	0.4	0.003	0.07	12	1.9	1850	0.07
2.0	1.00	1.2	0.010	0.20	37	5.6	1850	0.21
2.0	1.00	2.0	0.016	0.34	61	9.4	1850	0.34
2.0	1.25	0.4	0.003	0.04	10	0.8	1480	0.07
2.0	1.25	1.2	0.010	0.13	29	2.3	1480	0.21
2.0	1.25	2.0	0.016	0.22	49	3.8	1480	0.34
2.0	1.50	0.4	0.003	0.03	8	0.4	1230	0.07
2.0	1.50	1.2	0.010	0.09	24	1.1	1230	0.21
2.0	1.50	2.0	0.016	0.15	41	1.9	1230	0.34

A simple test was run to check the results of the calculation. The pressure drop was measured using a 0.95 m length of 1.5 mm diameter stainless steel tube, having a wall thickness of 100 μm. The tube was not insulated and so the coolant temperature at the outlet of the tube was generally several degrees higher than at the inlet. In many cases,

particularly for low flow rates, the coolant temperature was above –10 °C. The resulting data were then corrected to – 10 °C by factoring in the difference in fluid viscosity. The results are in reasonable agreement with the calculation, as seen in Figure 26.

4.7.3 Temperature of the Silicon

The main point is that even with thin insulating layers (epoxy, kapton) the large surface area of contact leads to more than adequate heat flow to keep temperature gradients very small. Rough calculations done so far, indicate that the silicon should hold to within a few degrees (less than 5) of the coolant temperature. The coolant temperature is not expected to have more than a few degrees rise in temperature from inlet to outlet of the layer. Hence, it will be possible to maintain the silicon at ~0 °C for a coolant temperature of –10 °C. Moreover, if desired, additional cooling could be obtained by use of the model B design with double the number of cooling channels.

4.8 Material budget

The design for Layer 00 that we have presented above places the layer at very small radius. In the interest of obtaining the best impact parameter resolution at low momentum, reducing the overall radiation in the detector, and to limit the deflection of the beampipe, we have designed Layer 00 in such a way that the material it adds is as small as possible. In this section we discuss the material budgets for the layer in the tracking region and in the forward hybrid regions. In both cases, the material sums are very low.

4.8.1 Central tracking region

We will use kapton cables to carry the signals from the sensors to the readout hybrids which will be positioned at approximately $\pm$ 40 cm from the center of the detector. This allows us to remove the mass, not only of the hybrids (~ 2 % X_o), but also of the cooling service lines that would be needed to carry the heat dissipated by the hybrids (~ 500 mW per SVX 3 chip). Figure 27 shows a schematic of the material layers in the regions away from the cooling tube for design A while Figure 28 shows the corresponding schematic in the cooling tube region. The material budgets for designs A and B are detailed in Table 7 for both regions. The region occupied by the cooling channels represents only about 15% of the total area of the layer in both designs. The total material added (i.e. not including the beampipe) by designs A and B outside the cooling regions is 0.574 and 0.465 % X_o, respectively.

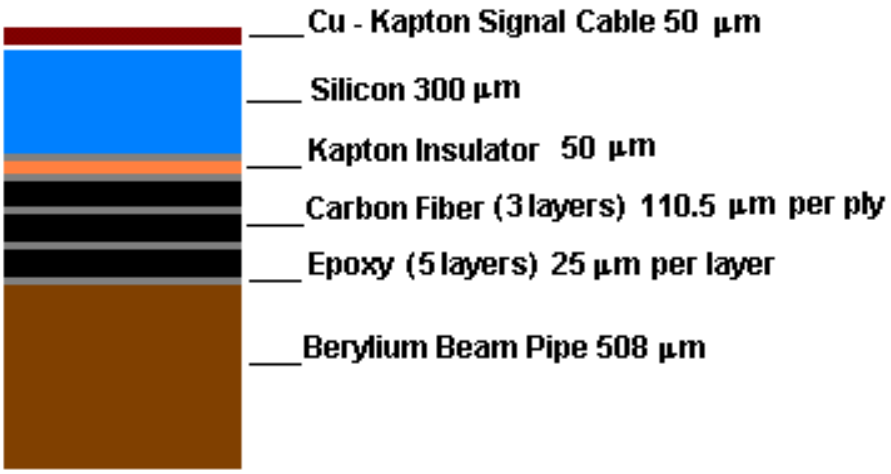

Figure 27. Material for model A where there are no cooling pipes.

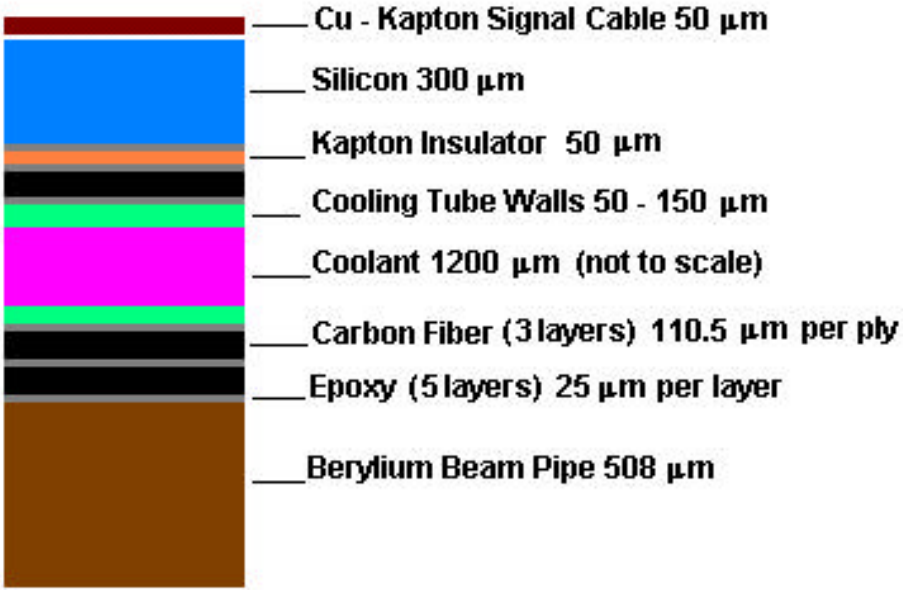

Figure 28. Material for model A where the cooling tubes are located.

Table 7 Material budgets for models A and B .

			Model A		Model B	
Layer & thickness	**Material**	**X_o [cm]**	**No Cooling**	**Cooling**	**No Cooling**	**Cooling**
Beampipe[††††] 508 μm	Be	35.4	0.14 % X_o		0.14 % X_o	
Film Adhesive 25 μm/layer	Epoxy	33.8	5 • 0.007 % X_o		2•0.007 % X_o	4•0.007 % X_o
C-fiber 110.5 μm/layer	Carbon & Epoxy	25.0	3 • 0.044 % X_o		0.044 % X_o	
Cooling Channel 150 μm/wall	Aluminum Alloy	8.9		0.171 % X_o		0.171 % X_o
Coolant 1200 μm	70 % H_2O 30 % Glycol	36.1		0.33 % X_o		0.33 % X_o
Insulator 50 μm	Kapton	28.4	0.018 % X_o		0.018 % X_o	
Sensor 300 μm	Silicon	9.4	0.32 % X_o		0.32 % X_o	
Signal Cable 50 μm	Kapton, Cu, Au, Ni	21.7	~3*0.023 % X_o		~3*0.023 % X_o	
Totals			**0.714**	**1.215**	**0.605**	**1.120**
Material added by Layer 00			**0.574**	**1.075**	**0.465**	**0.980**

4.8.2 Hybrid region

The hybrids are not yet designed, but are likely to be similar to the ISL hybrids. The ISL double-sided hybrids will be 3.7 % X_o if no effort is expended to reduce material.[25] This can be reduced to 3.08 % X_o by hatching the gold planes (which are the largest contribution). Of these values, only 0.596 % X_o is due to the substrate. The remainder is due to the multiple dielectric and conduction layers, and the components. To good approximation, we can reduce these contributions by a factor of two in estimating the total material in a single sided hybrid. We thus obtain a range of roughly 1.84 - 2.15 % X_o. To this we need to add the mass of the cooling collars. This will contribute somewhat more than the cooling channel in the tracking region. We estimate a value of order 0.5 % X_o. The total is therefore expected to be in the range of 2.3 – 2.7 % X_o.

4.9 DAQ

The Data Acquisition (DAQ) for L00 will be identical to the SVXII DAQ for all components downstream of the hybrids. However, the readout configuration differs from SVXII. It is chosen to minimize the DAQ cost while keeping the readout time less than the time for the SVXII readout, which occurs in parallel. The L00 ladders are single sided and shorter than the ladders in SVXII, so they should have on average about half as many hits to read out. This allows two ladders to be multiplexed. The multiplexing is done in Z i.e. the data from two ladders at the same ϕ but neighboring in Z are multiplexed onto a single readout path.

[††††] The beampipe braze joint is Aluminum Alloy and 3.6 % X_o. It covers only 0.8 % of the surface.

L00 & SVXII: Maximum R-ϕ Chip Occupation

5,000 Top Events at 2 TeV (<Min-Bias>=3, σ_z=30 cm):

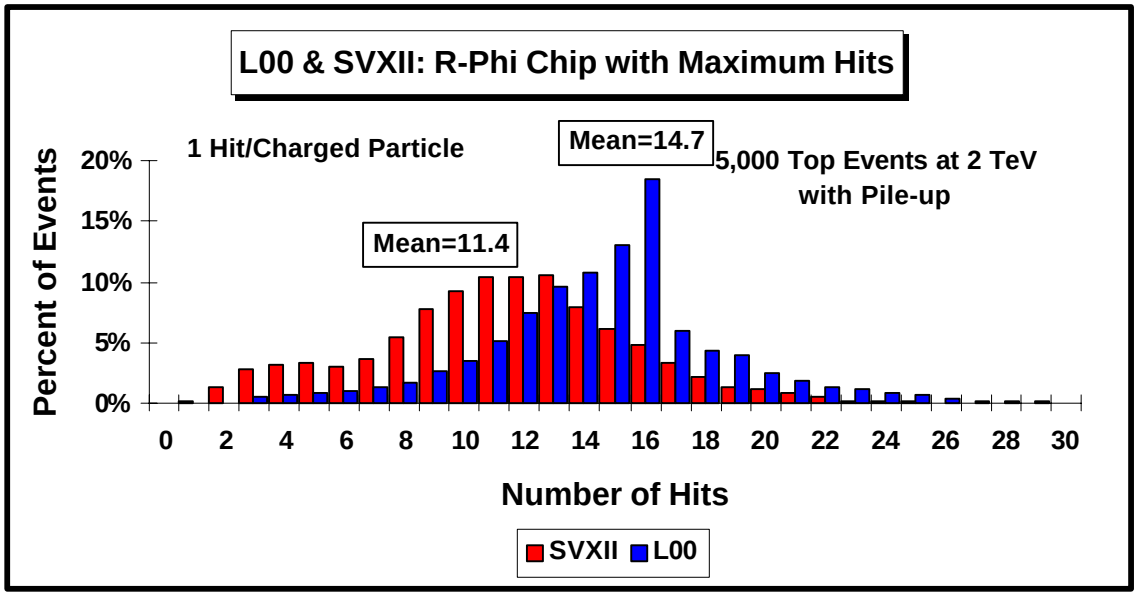

Occupation = 3 N_{hit}/128

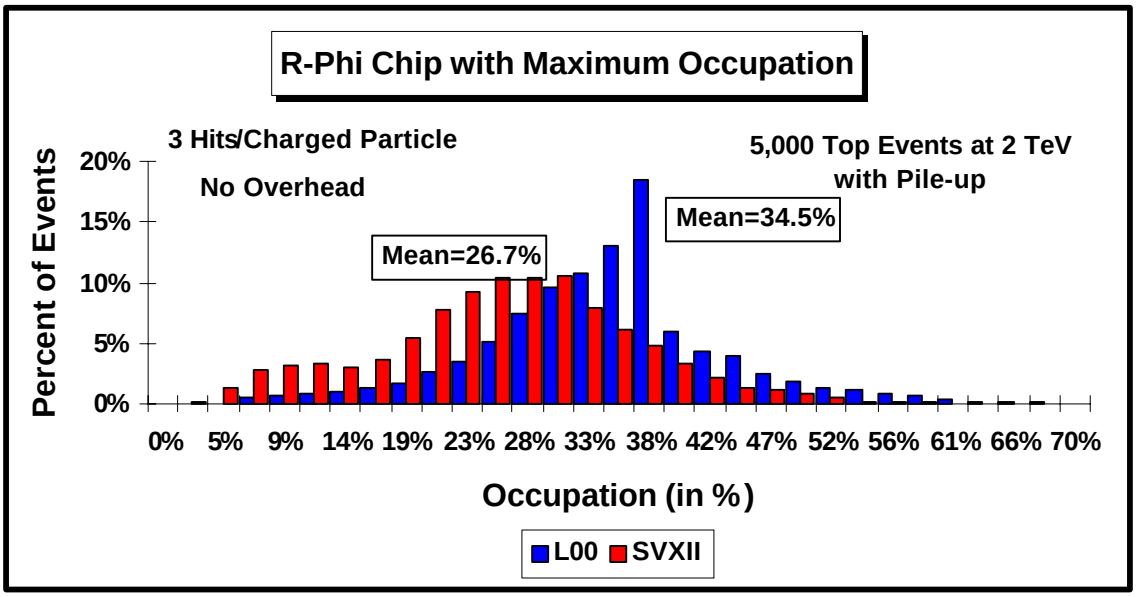

Figure 29. The upper plot shows the distributions of number of hits in the most occupied r-ϕ chip of L00 and SVXII. The lower plot shows the corresponding occupancy assuming that each particle occupies 3 strips.

SVXII & L00: Maximum Pathway Hits

5,000 Top Events at 2 TeV (<Min-Bias>=3, σ_z=30 cm):

With an added "overhead" of 1 hit per chip

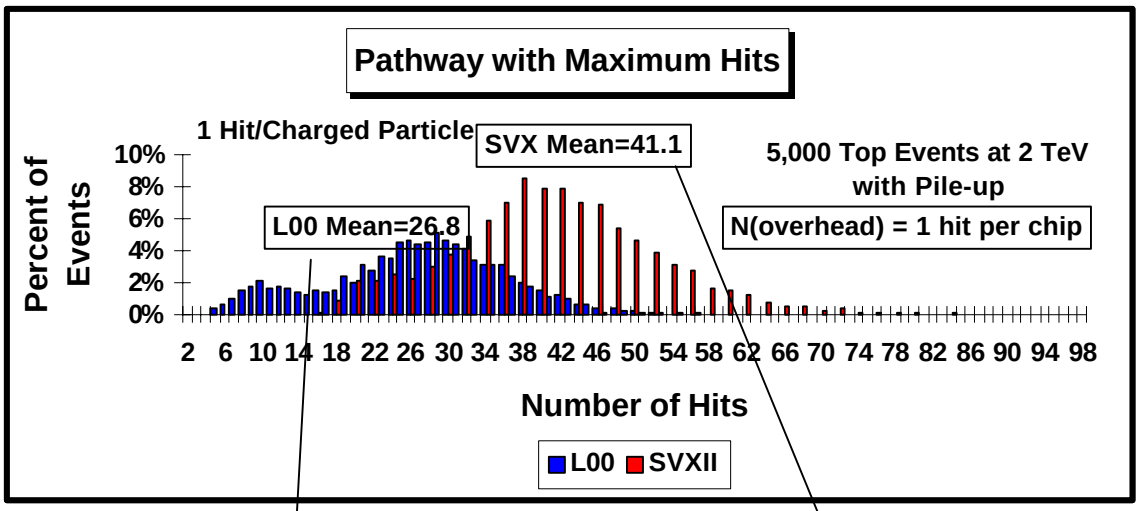

Nearest Neighbor Hits

3.2μs = 3*26.8/25MHz **4.9μs = 3*41.1/25MHz**

SVXII & L00: Maximum Pathway Readout Time

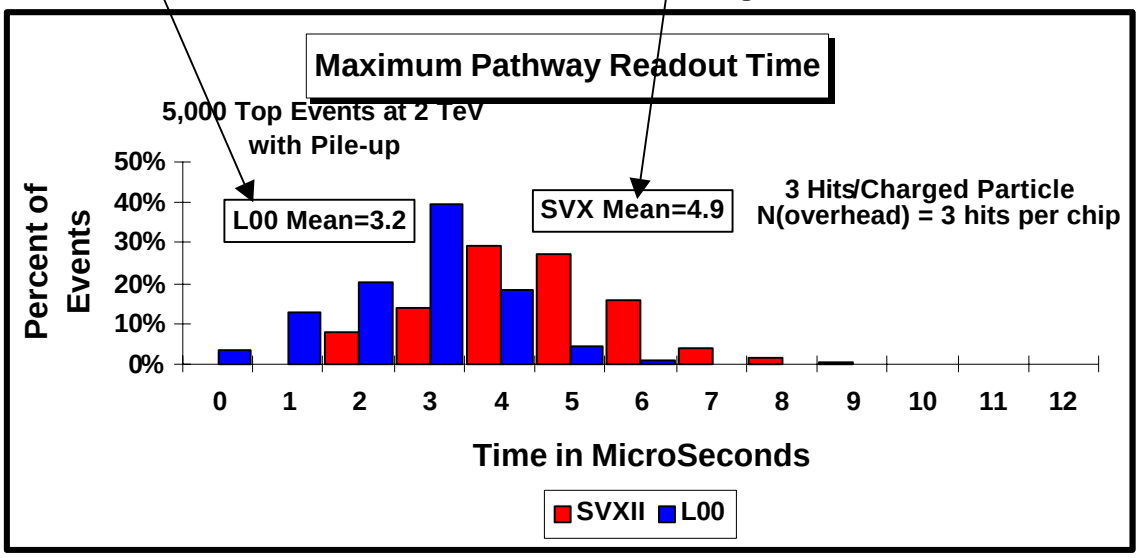

Figure 30. The upper plot shows the distributions of readout time for L00 and SVXII. A factor of 3 is included for nearest neighbor readout, and 3 channels per chip are added as overhead to simulate the effect of noise. The lower plot shows the difference in readout times. In about 90% of events, the L00 readout is faster than the SVXII readout.

4.9.1 Occupancy and Readout Time

The readout time is not driven by the average, but by the most occupied readout path. To account for this, a GENP level study was performed for the occupancy of L00, SVXII, and ISL which calculates the occupancies and readout times for the most occupied, and the average, readout paths. ISAJET is used to generate top plus a number of minimum bias interactions as determined by a Poisson distribution with a mean of 3. The Z of all interactions are distributed as a Gaussian with σ = 30 cm. The numbers of hits are recorded for each component of L00, SVXII, and ISL. The readout time of each readout path is calculated assuming that 3 strips are readout for each hit due to nearest neighbor latching. This is a bit of an underestimate especially for the 90 degree Z side strips in SVXII where up to twice as many strips could be readout per particle. However, this effect only increases the SVXII readout time relative to L00 and makes the following comparisons conservative for L00.

The first quantity of interest is the maximum occupancy, which is important for pattern recognition. Figure 29 shows the distribution of the *maximum* occupancy for L00 compared to SVXII i.e., the occupancy of the most occupied chip in each event. The L00 occupancies are slightly higher than SVXII as expected due to the smaller radius.

The other important quantity is the readout time, and in particular the readout time difference between L00 and SVXII. L00 is not used in the trigger, so it is only necessary to keep its readout time from introducing deadtime. The readout time is set by the readout of the most occupied readout path. Figure 30 shows the distribution of readout time for L00 and SVXII, and the distribution of the difference in readout time between L00 and SVXII ($\Delta t = t_{L00} - t_{SVXII}$). For 90% of the events, L00 finishes readout before SVXII. As mentioned above, the SVXII readout time is underestimated because of the treatment of the 90 degree Z side strips. It is estimated that this effect will increase the SVXII readout time by 20%. Incorporating that effect would increase the fraction of events for which L00 finished readout before SVXII to 97%. Given this result and the existence of 4 readout buffers, L00 should not introduce any deadtime.

4.9.2 Portcards

L00 would use the same portcard design as SVXII and ISL. It would require an additional 8 portcards beyond the 102 needed by SVXII and ISL. Four L00 portcards would be situated on each end of the detector. Due to the number of SVX 3 chips in L00, each portcard would have only 4 of the 5 available channels (HDIs) active on each portcard. The remaining channel can be left unstuffed and turned off. The best place to mount the portcards is on the ISL portcard ring, which is attached to the end of the ISL spaceframe, as shown schematically in Figure 1. In this configuration, the HDI cables connecting the hybrids and portcards would be about 70 cm in length. This is to be compared with 30 cm for SVXII and 120 cm for ISL. If the length of the cables is determined to be excessive, a fallback configuration is to mount the portcards in the SVXII spacetube just outside the SVXII barrels in Z. This approach would require modifications to the current SVXII installation procedure.

4.9.3 Cabling

The current SVXII designs for the flex cable, which brings power and control signals to the portcard, would be applicable to the L00 portcards as well. In addition, the junction card which mates that flex cable to the 30 degree slot cables can use the same design as SVXII. L00 would require two additional slots per end in the 30 degree crack for cables. Each slot would carry the low voltage and bias supplies for two portcards as well as the DOIM readout fibers. Four control cables per end would also be needed. These cables are very small, however, and could be routed through space left over in the SVXII and ISL slots devoted to that cable type.

4.9.4 FIBs

Two FIBs are needed per end. (Each FIB services two portcards). One FIB could be placed in each of the SVXII FIB crates per end. (There is also plenty of space for more FIBs in the ISL crates, but the associated power supply crates are full, so it is better to associate the L00 FIBs with the SVXII FIBs.)

4.9.5 Power supplies

L00 can use the same power supplies as SVXII with one modification. The SVXII power supplies are specified to have a maximum bias voltage of 200 V. Due to radiation damage, L00 may require a bias voltage above this level by the end of Run II. The L00 supplies would need to be modified to accommodate this higher voltage. Fortunately, the CAEN supplies are designed with daughter cards providing each of the different voltages needed. So, this modification involves only a single daughter card. The power supply modules for L00 low voltage and bias supplies can be mounted in the two free slots which are available in the power supply crates associated with the SVXII FIB crates.

4.9.6 VRBs

L00 would require 4 VRBs. These could be distributed among the SVXII crates. As L00 is not to be used in SVT, no splitters are needed. The GLinks between the FIBs and VRBs can be made the same length as the SVXII and ISL Glinks, but simply bypass the splitters. The addition of one L00 VRB per SVXII VRB crate increases the estimated readout size per crate by 250 bytes, which should have a negligible effect on the readout time into level 3.

5. Construction

The basic construction of the half cylinders could take place on a cast of the beampipe or a pipe of similar dimensions and with similar sag properties. We intend to map the pipe on a precision CMM and make a cast to form a dummy pipe to be used for L00 construction.

5.1 Support Structure and Cooling

We will form cylindrical tubes into channels with a press. We then glue all parts in place using a CMM for precision. The beampipe shape would be that expected in its final

state (i.e. by supporting Layer 00 during construction in the same way as it will be supported in the final installed state).

5.2 Modules

A flat, stiff, plate with a thin kapton layer would be used. Four sensors and one hybrid group would be glued to the kapton using a simple micrometer adjustment fixture for precision strip alignments. The kapton would also carry conductors to set the back plane voltage of the sensors. After the silicon is placed and glued to the kapton, which is itself attached via tabs to the stiff base plate, the kapton cables can be glued to the detectors and hybrids one by one. Each cable would be wirebonded at both ends before the next cable is installed.

5.3 Installation of Modules

Once the modules are complete, they can be installed on the support structure. A fixture would be used to hold aluminum end pieces, which are pinned to the base plate during module construction. For installation, the end pieces are retained to hold the reference of the strips, but the base plate is removed. A stepper motor and encoder would be used to clock the modules into the proper ϕ location. The module can then be glued to the support structure and later, the end pieces can be removed by cutting the kapton to which they are glued.

5.4 Construction Tolerances and Measurement of Final Positions

With equipment available at the Fermilab Si Detector Center, (SIDet) and based on past construction experience, we estimate that detectors can be aligned within modules, and from module to module in the support structure, to ± 25 μm. Using available large CMM's, it should be possible to map sensor locations relative to one another in 3 dimensions to better than ± 10 μm. We do not expect these positions to be stable. This is discussed in more detail in section 6 below.

5.5 Protective screen

A thin kapton screen with a thin conductive layer will be used to surround L00. The screen can be attached to L00 or it could be installed on the inside of SVXII. The screen can also serve to protect SVXII during beampipe installation.

6. Installation in SVXII

The installation of the beampipe would follow procedures similar to those already planned in the absence of Layer 00. The clearance between Layer 00 and SVXII is adequate for installation, especially if performed on the bed of a large CMM such as the Browne and Sharpe, 3 m CMM at SiDet. We anticipate no difficulties so long as the beampipe is not accidentally struck. Special precautions will be taken to avoid such accidental deflections during installation. After installation the pipe can be rigidly supported at a number of points. We have found some configurations that attenuate

deflections that initiate at the ends of the beam pipe by 3 to 4 orders of magnitude by the time they reach the central region.

6.1 Alignment, Position Monitoring

The precision by which L00 measures track positions exceeds the precision by which the sensors can be positioned within SVXII. Although the position of L00 sensors relative to one another can be measured using a coordinate measuring machine with a precision approaching the detector resolution, no such measurements are possible once the detector is inserted into SVXII. With the placement of L00 determined entirely by a relatively imprecise installation procedure, it becomes critical that track data alone be sufficient to determine the detector alignment to a precision comparable to the intrinsic resolution.

In the most basic analysis, the procedure and expected precision for a track-based alignment of L00 is the same as that for any other layer in the detector. The success of track-based alignments of SVX and SVX' in Run I suggests that similar algorithms will succeed for the Run II silicon detectors. Indeed, for SVXII, the larger detector overlaps, better initial alignment and significantly better Z resolution than was available for the Run I detectors holds open the prospect of a greatly improved outcome. There are, however, several significant differences between L00 and the other layers in SVXII that may influence the result and merit some discussion. The dissimilar wedge geometry, the unaligned initial state, and the mechanical independence of SVXII and L00.

The azimuthal size of L00 modules is larger than that of wedges in SVXII. This difference has at least two consequences. First, tracks that pass through a single L00 sensor illuminate more than a single wedge in SVXII. Second, the range of incidence angles (in azimuth) on the detector is larger than it is for detectors in SVXII. At best, both of these differences improve the determination of detector alignment, and at worst, make no difference. In general, elements that link adjacent SVXII wedges together help to reduce relative misalignments. The persistence of significant wedge-to-wedge misalignments in SVX and SVX' were due in part to the lack of such wedge-spanning detector elements. Initially, the complication of linking wedges together can be ignored; in which case we recover the simple, single-ladder alignment problem. Similarly, increasing the range of incidence angles improves the sensitivity to misalignments that change the radius of the sensors (including rotations).

After installation, it is conceivable that the position of strips within L00 relative to those in SVXII may be more than 200 μm from nominal. Such a large misalignment may significantly hamper proper association of hits within L00 to tracks through the rest of the silicon. The solution to this problem is to start with a sample of low multiplicity events in which the hit associations can be made with a reasonable degree of accuracy. A small sample of such events, even if reconstructed by hand, should suffice to establish the alignment at the level of ±30 μm or better. Although misalignments at this level may affect the pattern recognition, experience with SVX and SVX', which were aligned to no better than 20 -30 μm initially, shows that the pattern recognition finds the majority of tracks in sparse events with sufficient accuracy to allow alignment via an automated algorithm.

The mechanical independence of L00 from SVXII poses the most serious risk to the success of a track-based alignment. The SVXII spacetube, like the ISL spaceframe, is designed to isolate the detectors from incidental forces that may develop during the installation process, handling of cables, etc. To a good approximation, the spacetube is mounted in a stress-free state in the ISL. In contrast, L00 is connected directly to the beampipe, which in turn is connected to the SVXII spacetube, the ISL spaceframe and a number of other detector elements. This situation opens the possibility of allowing incidental forces, perhaps from sources outside the tracking region, to move L00. Even worse, the coupling between the pipe and the spacetube and spaceframe might compromise the mechanical isolation of those systems, thereby allowing the same forces to move the other silicon detectors as well. Finally, temperature dependent effects, mechanical vibrations coupled to the beampipe, or other time dependent forces could alter the detector position on a time scale sufficiently short that the data collected during any single position state proves inadequate to determine the alignment.

The solution to these problems is to design the beampipe support to decouple motions induced at the end of the pipe from those at the center. In order to prevent movement of the ISL, the forces transmitted to the pipe at the low-profile flanges must be transferred directly to the end of the ISL extension tube, and thereby to the COT endplate. Care should be exercised to ensure that any vibrations transmitted to the corrugated beampipe be damped prior to reaching the Be pipe. Foam wadding, or other suitable damping material placed around the beampipe in the 3° hole would likely suffice for this purpose. We currently possess quite accurate mathematical models for the behavior of the spaceframe and spacetube. These tools can be used to test and develop various design concepts and help define the required specifications for the beampipe mounting system. Preliminary analyses presented in the next section indicate that good vibration isolation can be obtained.

6.2 Vibration and Stability

To make use of the excellent position resolution of the Layer 00 sensors, it is important that they do not move after installation of the Layer in the silicon tracker. The beampipe is coupled in z to a bellows style pipe that can be easily damped. The beampipe supports will couple to the central track system, which has been a stable object in past runs. Nevertheless, the high precision of Layer 00 sensors make them more sensitive to position instability. An engineering study was therefore performed to illuminate the vibrational characteristics of Layer 00. Three different beampipe support configurations were considered and a sinusoidal driving force was assumed. The force displaced the end of the beampipe in the transverse direction with amplitude of 1 mm. In each case, the resulting displacement at three positions along Layer 00 was determined. Ratios of the displacements at these locations to the initial displacement at the end of the beampipe, was plotted as a function of frequency from 10 Hz to 10 kHz. The three beampipe support configurations were as follows:

1) Supports at the COT face and the end of ISL only
2) Add supports between the SVXII barrels
3) Add support at the end of SVXII

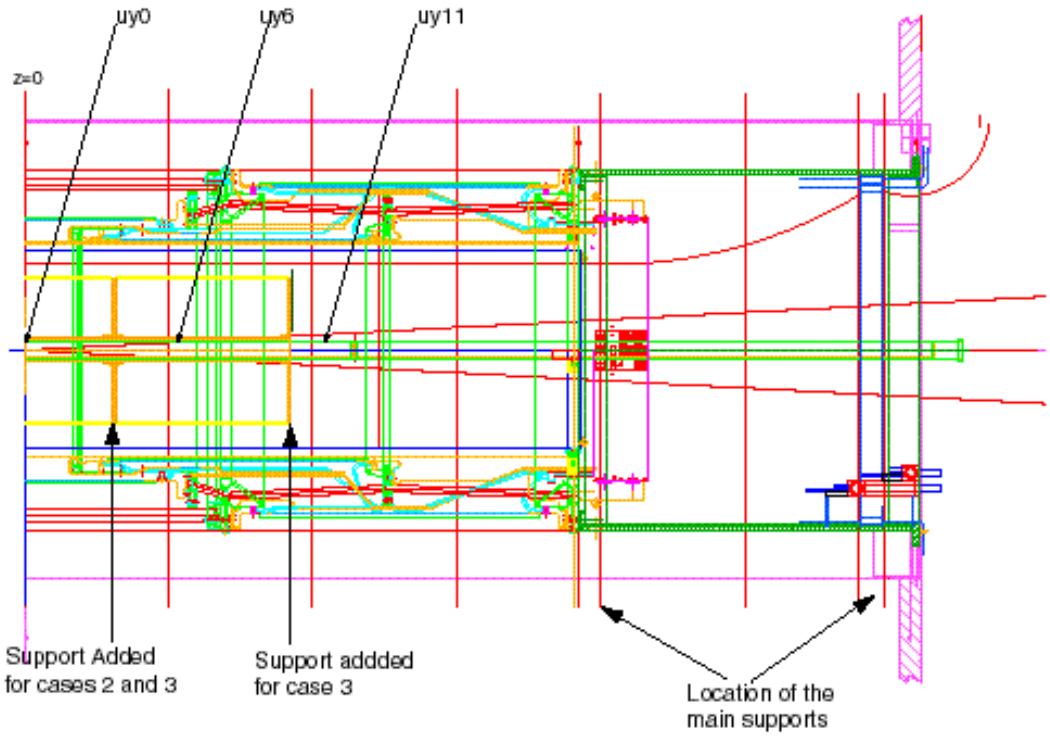

Figure 31. One half of the silicon track system showing the locations of beampipe supports used in the vibrational analysis. Also shown are the locations uy0, uy6 and uy11, where the displacement ratios were calculated.

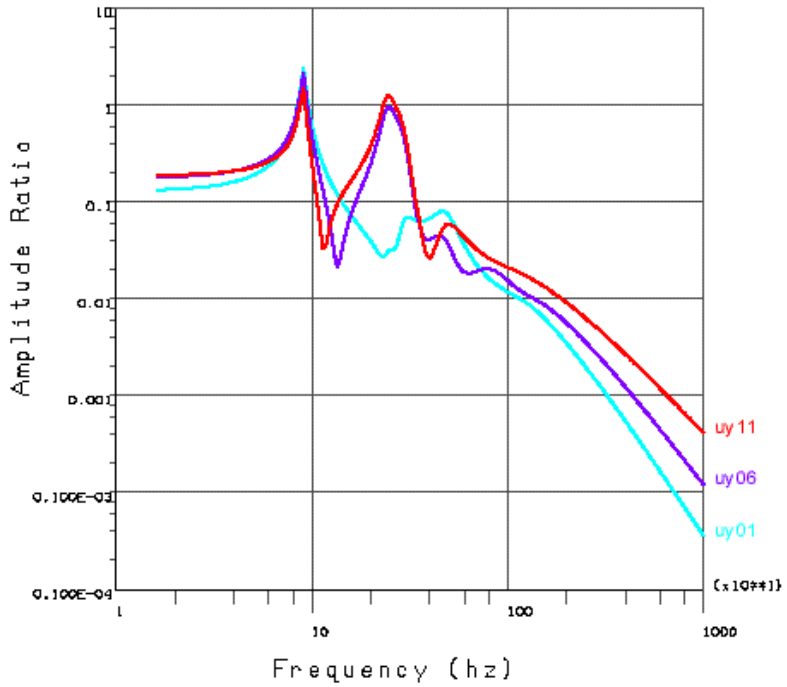

Figure 32. First case: beampipe supported only at the ISL and COT end flanges. The plot shows the transverse displacement attenuation factor versus frequency (x10) for a beampipe deflection initiated at end of Beryllium section. Uy01 is the ratio expected at z = 0. Uy06 and Uy11 are at 15 and 35 cm, respectively.

The locations where the ratios of displacements were determined were at z = 0, 26, and 51 cm. These locations and the support locations for the various cases are shown in Figure 31. The results for the three cases are plotted in Figure 32, Figure 33, and Figure 34. The natural frequencies of the system appear to be at roughly 100 and 200 Hz. Without additional supports, (case 1) there is no attenuation at Layer 00 at these frequencies. As supports are added, attenuation of several orders of magnitude can be seen. Ultimately a 1 mm displacement of the end of the beampipe is seen to result in less than 1 μm displacement at the center of Layer 00. If needed, we could add supports at the end of the SVXII barrels. The supports would be in the form of wire spiders similar to those used in Run I but would need to be installed after the installation of Layer 00 when the regions of SVXII are inaccessible. This could be achieved by pre-threading wire through eyelets in the SVXII spacetube. The wire could extend along the outside diameter of the spacetube and out to the end of the silicon detector.

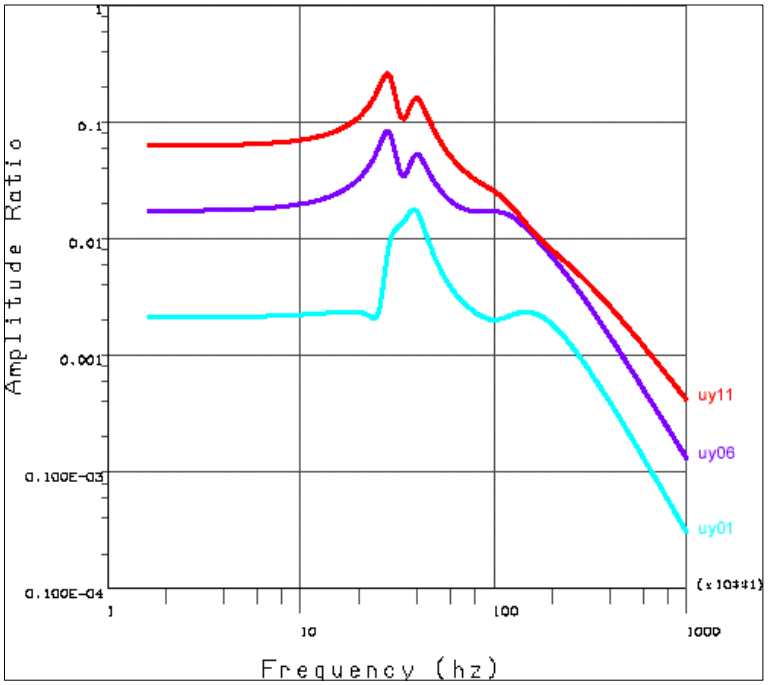

Figure 33. Second case: Add support between SVXII barrels.

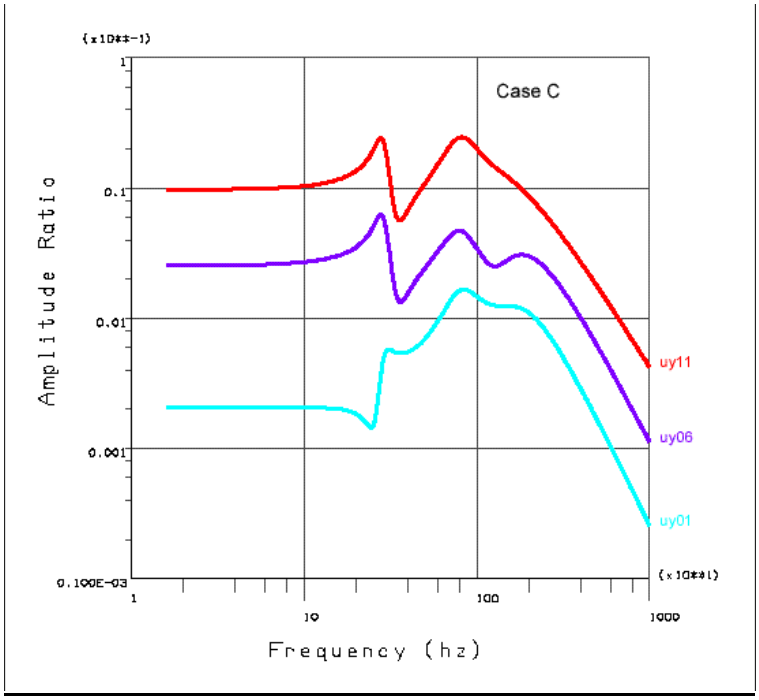

Figure 34. Third case: add a support at the end of SVXII. Note that the horizontal scale is x 10 while the vertical scale is x 10^{-1}.

7. Schedule and Cost

We estimate manpower at 2 FTE technician for 6 to 9 months. Material costs are not high. Silicon will cost 75k$. CMS has already paid the cost of prototyping detectors specifically designed for use in CDF Layer 00. This saved on the order of 40k$. Lightweight cables are conservatively estimated at 87k$. Hybrids should not be more than 75k$. Modification of the beampipe to a smaller radius would greatly simplify construction and installation. We have received a quotation for 39 k$ for this. All other materials are cheap except DAQ components. We would hope to use spares from SVXII and ISL. Note that the spare fraction for SVXII and ISL is roughly 10% of that used. The requirements for Layer 00 are of order 5 % of SVXII + ISL. Purchased new, all DAQ components would cost 288k$. (Many if not all of these components could be made up of spares at no new cost.) The total cost of Layer 00 including all DAQ items would be on the order of 500k$. Total construction and installation time would be relatively short. Layer 00 could be ready for the start of Run II.

8. Conclusion

Layer 00 would significantly improve the CDF tracking system in regard to nearly every major physics goal of the collaboration. It would also provide some insurance against the loss of SVXII inner layers while providing us with important experience for preparing a Run III upgrade. It is possible to complete the project in time for the start of Run II. The cost would not exceed ~500k$. We believe that work should start as soon as possible.

Acknowledgements

We would like to acknowledge N. Delerue (FNAL summer student from Paris Sud University) for his enormous help in putting together the tools used in our physics studies of b tagging. Similarly, we thank B. Edwards (FNAL summer student from Rice University) for his very careful measurements of the ambient heat load on Layer 00 as obtained with a scale mock up he constructed. We gratefully acknowledge FNAL engineers G. Derylo (studies of small cooling channels - section 4.7.2), and Z. Tang (beam pipe vibration calculations – section 6.2) for their calculations and tests. We thank R. Field for his detailed study of the occupancy and readout times of Layer 00 (section 4.9). We would also like to thank D. Benjamin, I. Dunietz, K. Einsweiller, B. Flaugher, R. Kephart, J. Spalding, and Paul Ratzmann for their comments and assistance.

References

[1] CDF Collaboration, D. Amidei ed., *CDF Upgrade Technical Design Report*, CDF 3777, (1996).
[2] J. Albert et al., *The Relationship Between SVX Signal-To-Noise and B Tag Efficiency,* CDF 3338 (1995).
[3] M. Frautschi, *Radiation Damage Issues for the SVX II Detector*, CDF 2368 (1994).
[4] J. Matthews, *Effective Si Damage Fluences Measured by SVX and SVX´*, CDF 3937, (1996)
[5] D. Amidei et al., *Study of CDF II for Tev33,* CDF 4370, (1997).
[6] J. Conway et al., *The Status of Diamond Detectors and a Proposal for R&D for CDF Beyond Run 2*, CDF 4233, (1997)
[7] CMS tracker TDR, to be released June 1998.
[8] G. Tonnelli et al., NIM A377(1996) 422
[9] A. Chilingarov et al., ATLAS inner detector group, NIM A360 (1995) 432.
[10] G. Bolla, *Pixel 98,* May 8,1998 at FNAL, new results were presented for single-sided n on p silicon with depletion voltage of 100 V in which 100 % charge collection efficiency was obtained after a proton dose of 27 Mrad.
[11] E. Fretwurst et al., NIM A342 (1994) 119-125.
[12] See, for example, F. Dejongh, *Proper Time Resolution for B_s Decays in Run II,* CDF 4475, (1998) and F. *CDF Sensitivity to B_s Mixing in Run II,* CDF 4362, (1997).
[13] This study was performed by T. Meyer, (Currently at Cornell University), while a summer student at FNAL in 1995.
[14] R. Culbertson, FITS program to calculate IP resolution for various geometrical configurations, hit resolutions and material distributions in silicon microstrip detectors.
[15] R. Snider and J. Incandela, *Effect of material on SVXII impact parameter resolution*, Talk presented to the CDF Upgrade meeting Jan. 9, 1998 (available at the website: http://www-cdf.fnal.gov/internal/upgrades/svxii/Mechanical/Mass/mass.html). CDF note in preparation.
[16] R. Culbertson, *Optimizing SVX´ Track Selection*, CDF 2982 (1995)
[17] N. Bacchetta et al. **,** *Proposal for Intermediate Radius Silicon Layers for CDF, CDF 3829 (1996)*
[18] See http://www-cdf.fnal.gov/internal/upgrades/svxii/Mechanical/thermal.html and references therein.
[19] *Report of the Tev2000 Study Group on future electroweak physics at the Tevatron*, D. Amidei and R. Brock, editors, Fermilab, 1995
[20] J. Spalding, private communication.
[21] G. Gandi, CERN microcable laboratory.
[22] Z. Tang, Fermilab Engineering Group.
[23] K. Y. Ng, *Power Loss to Tevatron Beampipe*, FERMILAB-TM-2015 (1997)
[24] See for instance, W.M. Rosenaw, *Handbook of Heat Transfer Fundamentals, 2nd ed.*, (McGraw-Hill, New York) 1986
[25] All estimates for ISL hybrids are based on the material budgets as of 2/26/98.